Optical Fiber Technology 19 (2013) 741–759

Contents lists available at ScienceDirect

Optical Fiber Technology

www.elsevier.com/locate/yofte

Invited Paper

Gas detection with micro- and nano-engineered optical fibers

W. Jin *, H.L. Ho, Y.C. Cao, J. Ju, L.F. Qi

Department of Electrical Engineering and Shenzhen Research Institute, The Hong Kong Polytechnic University, Hong Kong, China

ARTICLE INFO

Article history:
Available online 19 September 2013

Keywords:
Optical fiber gas sensors
Optical fiber sensors
Microstructured fibers
Hollow core fibers
Suspended core fibers
Photoacoustic spectroscopy

ABSTRACT

This paper overviews recent development in gas detection with micro- and nano-engineered optical fibers, including hollow-core fibers, suspended-core fibers, tapered optical micro/nano fibers, and fiber-tip micro-cavities. Both direct absorption and photoacoustic spectroscopy based detection schemes are discussed. Emphasis is placed on post-processing stock optical fibers to achieve better system performance. Our recent demonstration of distributed methane detection with a ~75-m long of hollow-core photonic bandgap fiber is also reported.

1. Introduction

Optical fiber technology is playing an increasingly important role in environmental and safety monitoring, as well as chemical and biological sensing. They are based upon different sensing mechanisms such as absorption [1–3], Raman scattering [4–6], fluorescence [7,8], surface plasmon resonance [9–11], and mechanical-deformation caused by gas-material interaction [12,13]. There are pros and cons associated with sensors based on different mechanisms [14–17]. This paper focused on fiber sensors based on direct absorption and photoacoustic spectroscopic principles, which have been studied extensively recently for its simplicity, high sensitivity, multiplexing capability, and greater potential for field applications.

There have been considerable efforts in developing absorption-based fiber-optic systems for gas detection and recent researches are directed toward developing systems with higher sensitivity, faster response time, wider coverage of gas species, and distributed sensing capability. A number of sensor structures, system configurations and signal detection techniques have been developed and successfully employed. They vary significantly depending on their desired characteristics and applications. Conventionally, fiber optic gas sensors are based on measuring the optical absorption at specific wavelengths with an open-path absorption cell comprising a pair of collimator lenses with fiber pigtails. The optical fiber here just performs a purely passive role in transferring light to and from the absorption cell but plays no part in gas sensing. The sensitivity of such sensors can be improved by increasing absorption path length. However, the improvement is limited because of the difficulty in fabricating a long absorption cell. Very long optical path lengths may be achieved by using multi-pass optical cells such as the White cells [18] or Herriott cells [19]. However, these gas cells are bulky, expensive and unsuitable for field applications. Gas detection by evanescent field absorption has been demonstrated with a D-shaped optical fiber (D-fiber) [20] and a single mode fiber (SMF) with a small hole at the center of the core [21]. Such fibers offer the possibility of extra-long interaction length and potentially distributed sensing. However, they suffer from relatively low sensitivity as compared to open path sensors due to the very little optical power fraction available for light and gas interaction.

Microstructure optical fibers (MOFs) are a novel class of optical fibers that appeared since 1990s [8]. MOF family includes index-guided photonic crystal fibers (IG-PCFs), hollow-core photonic bandgap fiber (HC-PBGFs), and suspended-core fiber (SCFs). These fibers offer novel optical properties including extended single- [22,23] and two-mode [24] wavelength range, unusual dispersion characteristics and enhanced non-linearity [25–27], and light guiding in an air-core [28]. The special holey structure of MOFs opens up new possibilities for novel sensing applications by exploiting light and matter interaction within the hole-columns. Gas detection based on absorption spectroscopy with IG-PCFs was proposed by Monro et al. in 1999 [29] and experimentally demonstrated by Hoo et al. in 2002 [30]. Afterwards, numerous designs and configurations of MOF based gas sensors have been reported [31–35], aiming to develop sensors with better sensitivity and distributed detection capability.

In the meanwhile, efforts are being made to develop fiber-optic gas sensors based on photoacoustic spectroscopy (PAS). Early PAS systems use optical fibers to deliver light to photoacoustic (PA)

* Corresponding author.
E-mail address: eewjin@polyu.edu.hk (W. Jin).

1068-5200
http://dx.doi.org/10.1016/j.yofte.2013.08.004

cells to excite acoustic waves, while the detection of the acoustic wave is performed by electro-mechanical transducers [36–38]. Recently there have been reports in developing optical and fiber-optic means to probe the acoustic wave [39–41]. The use of optical fibers for excitation as well as detection of the PA pressure wave makes it possible for remote and multi-point gas detection in a multiplexed fiber-optic sensor network.

In this article, we start with a brief overview of the foundations of absorption spectroscopy and PAS, and a review of past development on gas detection using optical fibers; then discuss current researches on absorption-based gas sensors with SCFs, HC-PBGFs, as well as fiber gas sensors with PAS; and look into potential further development in distributed and multiplexed fiber-optic gas detection systems.

2. Direct absorption spectroscopic gas detection with optical fibers

2.1. Open-path sensor

Optical methods for the identification of chemical species including gases are well known [42] and were widely used long before the advent of optical fibers. Most of these techniques are based on measurement of radiation absorption by the chemical species. The characteristic absorption spectra can be used as "finger print" to identify different chemical species. The experiments in the early part of this century by Planck, Bohr and Einstein showed that the energy of a microscopic system such as an atom or a molecule is quantized [1]. In a certain approximation, we may resolve the total energy of a molecule into the sum of electronic, vibrational, and rotational energy [42]. Transitions between different energy levels can take place by either energy absorption or emission. Corresponding to different type of transitions, the molecular absorption spectra can be classified into four categories [43]: rotational spectra, vibrational spectra, vibrational–rotational spectra and electronic spectra. Many gas molecules have absorption lines in the low loss transmission window of the silica fiber, i.e., 0.8–1.8 μm, corresponding to vibrational or vibrational–rotational transitions. The absorption wavelengths and line strength of some common gases are listed in Table 1.

The strength of gas absorption lines can be used to perform quantitative measurement of gas concentration. For light of intensity I_o incident on a cell of length l containing a chemical species which has an absorption line or band at specific wavelengths, the output intensity I is given by the Beer–Lambert law [42]:

$$I = I_0 \exp[-\alpha l C] \tag{1}$$

where α is the absorption coefficient and is proportional to the line strength, and C is the concentration of the sample gas (see Fig. 1). The absorbance of the sample is defined as [43]

Table 1
Absorption wavelengths and line strength of some common gases [44,45].

Gas	Absorption wavelength (nm)	Line strength (cm^{-2} atm^{-1})
Acetylene (C_2H_2)	1533	$\sim 20 \times 10^{-2}$
Hydrogen iodide (HI)	1541	0.775×10^{-2}
Ammonia (NH_3)	1544	0.925×10^{-2}
Carbon monoxide (CO)	1567	0.0575×10^{-2}
Carbon dioxide (CO_2)	1573	0.048×10^{-2}
Hydrogen sulfide (H_2S)	1578	0.325×10^{-2}
Methane (CH_4)	1667	1.5×10^{-2}
Hydrogen fluoride (HF)	1330	32.5×10^{-2}
Hydrogen bromide (HBr)	1341	0.0525×10^{-2}
Water (H_2O)	1365	52.5×10^{-2}
Oxygen (O_2)	761	0.019×10^{-2}
Nitrogen dioxide (NO_2)	800	0.125×10^{-2}

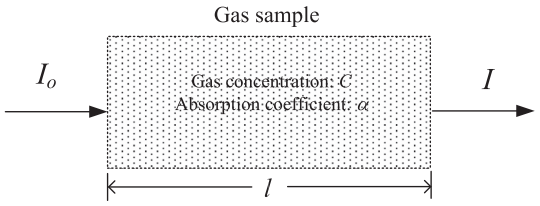

Fig. 1. Principle of absorption spectroscopy.

$$A = \log\left(\frac{I_0}{I}\right) = 0.434\alpha l C \tag{2}$$

The absorbance is linearly proportional to α, l and C; and can then be used to obtain gas concentration C if the cell length l and the absorption coefficient α are known.

The use of wavelength modulation spectroscopy (WMS) significantly enhances the signal-to-noise ratio (SNR) since the noise at frequencies other than that of the reference is rejected [46]. Fig. 2 shows the basic principle of WMS. A sinusoidal modulation is impressed onto the optical wavelength of a narrow line-width light source while the center wavelength is slowly ramped over the absorption line of interest by for example temperature tuning. The signal output is processed by, in general, a lock-in or harmonic detector referenced to the modulation frequency. The absorption strength (thus the gas concentration) is proportional to the amplitude of the second or first harmonic signal.

A typical open path gas cell uses a pair of pigtailed graded index (GRIN) lenses to collimate the output light from the input fiber, and collect the light back into the output fiber. Interaction between light and gas takes place at the space between the lenses. Fig. 3a shows a home-made fiber-optic open path cell with an absorption path length of 25 mm. With such a cell, a detection sensitivity of 75 ppm acetylene was achieved [47]. Reflections at the GRIN lenses' surfaces and the lens/fiber joints were found to induce unwanted interference signals due to etalon effect, and WMS with appropriate modulation amplitudes [48] combined with wavelength scanning has been identified to be an effective method to minimize such unwanted signals [48–50]. Morante et al. proposed a novel micro-optic cell by employing a pair of GRIN lenses with a pitch of 0.264 [51], and with such a cell, back-reflected light from the lenses become highly divergent and the etalon effect is effectively reduced.

To achieve a higher detection sensitivity, Sa et al. and Ho et al. proposed to use cascaded GRIN lenses to increase the effective absorption path length [52,53]. The latter fabricated a gas cell by cascading 10 pairs of fiber pigtailed GRIN lenses fixed to a circular metallic frame with an inner diameter of 10 cm. The insertion loss of such a gas cell is less than 8 dB. By connecting six such cells in serial, a super gas cell with an overall absorption path length of 6 m was built (Fig. 3(b)) and was used for detecting multiple gases for fault monitoring in oil-filled transformers [53]. Recently a compact reflective gas cell was constructed by Liu et al. for which a pair of GRIN lenses and a pair of flat-bottomed glass blocks with highly reflective coating were used [54]. The distance between the glass blocks is 2 cm and the effective absorption path length of this reflective gas cell is 30 cm with an insertion loss of ~1.5 dB. .

2.2. Evanescent wave gas sensor

Evanescent wave (EW) gas sensors refer to where light-gas interaction occurs within the evanescent field region of the optical fiber. In this case, the optical fiber plays the most direct role in the sensing process and the characteristic equation of the sensors may be re-written as [55,56]

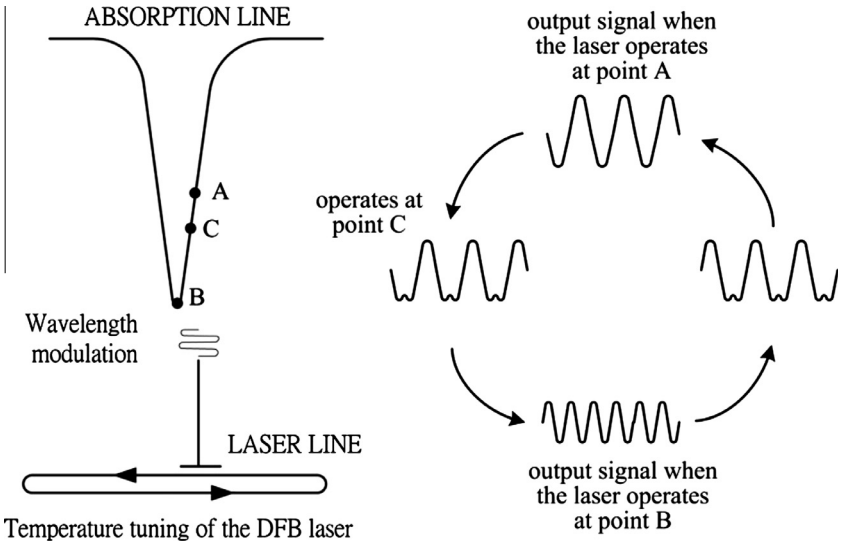

Fig. 2. Principle of wavelength modulation spectroscopy with a scanning approach.

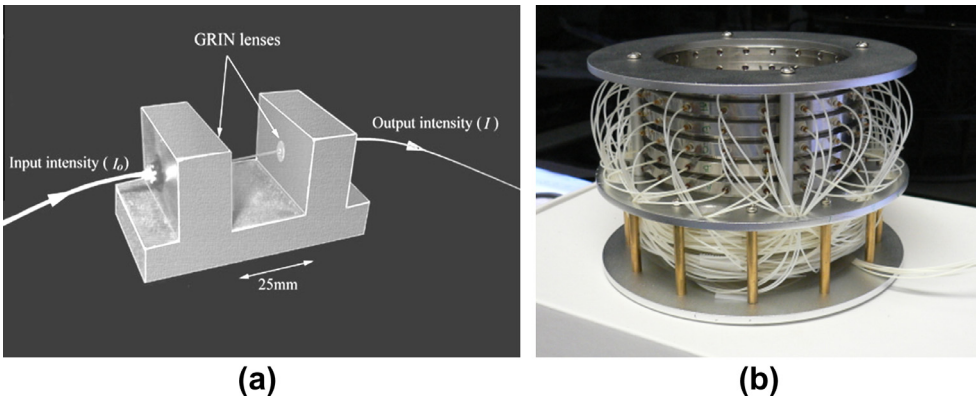

Fig. 3. (a) A 2.5 cm long open path gas cell and (b) a 6 m long gas cell made by cascading 60 pairs of fiber-pigtailed GRIN lenses.

$$I = I_0 \exp[-r\alpha lC] \tag{3}$$

where r is the relative sensitivity with respect to direct absorption for the same absorber with the same length. r in Eq. (3) is defined as [57]

$$r = (n_r/n_e)f \tag{4}$$

where n_r is the index of the gas species and is approximately equal to 1. n_e is the effective index of the guided mode. f is the fraction of the total EW power that interacts with gas. Typical EW sensors use side-polished fibers, tapered micro/nano fibers and D-fibers as illustrated in Fig. 4; as well as IG-PCFs and SCFs.

Side-polished fiber can be fabricated by polishing a curved SMF embedded in for example a quartz block (Fig. 4a). The cladding region on one side of the fiber can then be removed. The disadvantages of this sensor are its time-consuming fabrication process and difficulty to fabricate long length of side-polished fibers. Hussey et al. developed a wheel-polishing method, which allows the fabrication side-polished fibers with a length of several centimeters [58]. However, the fraction of EW power exposed to the environment is small and it is difficult to built high sensitivity sensors with such fibers.

Tapered optical micro/nano fibers (Fig. 4b) have received considerable attention recently. They are typically fabricated from a standard fiber by the flame-brushing technique [59,60] in which the fiber is stretched when it is heated with a stationary or an oscillating flame torch. The waist diameter of fiber tapers can be reduced down to less than one micrometer. The small diameter means that a considerable fraction of optical power is propagating outside the air/silica boundary in the form of EW. An early demonstration using tapered fiber for methane gas detection was performed at 3.3 μm, however, remote detection is not possible because of the large attenuation of silica fibers at this wavelength. Low loss bi-conical tapers with a submicron-diameter taper waist and a waist length of up to ~10 cm have been fabricated with the flame-brushing technique [59], and the EW power fraction can be over 20% around 1550 nm. However, the thin tapered region is not easy to handle, making it difficult to be used as practical sensors.

D-fibers (Fig. 4c) are drawn from a conventional preform but with half of the cladding region removed. This fiber allows continuous access to the evanescent field, thus very long interaction length. The use of D-fiber for gas detection has been demonstrated [61,62] but the sensitivity is very low, on the order of 0.01% that of the open path sensor of the same length. Calculation shows that the use of a high index overlay on top of the flat surface enhances the sensitivity but the improvement factor is modest, typically $\leqslant$10 [61,63].

IG-PCFs are made with a stack-and-draw process and they have a periodic array of air-holes running in the cladding region and light is confined to a solid core by modified total internal reflection

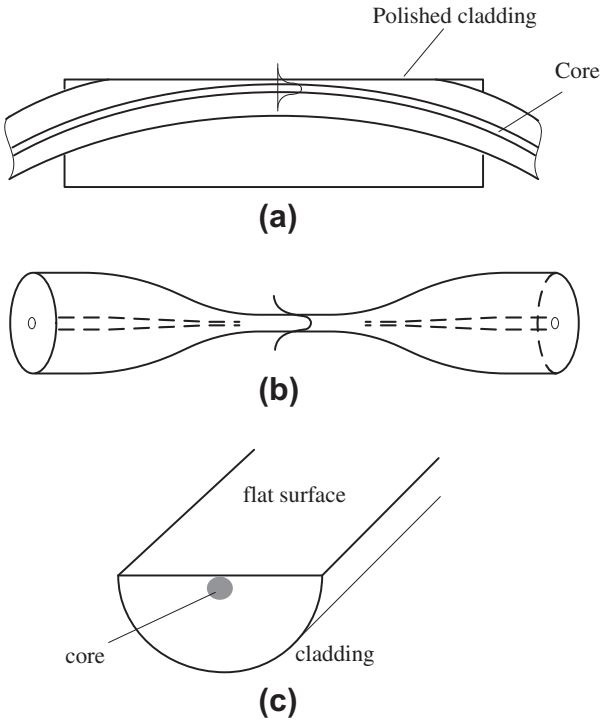

Fig. 4. (a) Side-polished fiber; (b) Tapered fiber; (c) D-fiber.

(M-TIR) from the reduced-effective-index cladding. A properly designed PCF has a significant fraction of EW located within the air-holes and hence can be a good platform to study light-gas interaction through EW.

The relative sensitivity r of an IG-PCF based gas sensor is affected by a number of parameters including operating wavelength λ, the core-size, the size d and pitch Λ of the air-hole array in the cladding. Fig. 5(a) shows the cross section of a particular IG-PCF. The relative sensitivity r as a function of wavelength is calculated by using Finite Element Method (FEM) and shown in Fig. 5(b). At wavelengths of 1.53 and 1.65 μm, corresponding to respectively the absorption lines of Acetylene (C_2H_2) and Methane (CH_4) gases, the relative sensitivities are respectively 12.6% and 14.9% that of an open path cell per equal length. This sensitivity is about 3 orders of magnitude higher than that of the D-fiber. Theoretical simulation shows that the relative sensitivity increases with the operating wavelength λ and relative hole size d/Λ, but decreases with structural size d or Λ (for the same d/Λ). There have been reported that specially designed IG-PCF could achieve a relative sensitivity as large as 30% [29,64].

Hoo et al. carried out the first experimental demonstration of gas detection with IG-PCF. We used 10 cm small core PCF with one end fusion-spliced to a SMF, while the other end is butt coupled to a second SMF with ~50 μm gap between the two fiber ends to allow for gas diffusion into the holes (Fig. 6). The fusion spliced end of the PCF is effectively sealed and the experimental system can be regarded as a diffusion system with a single open end.

Fig. 7 shows the measured normalized minimum transmittances as functions of time when the source wavelength is tuned to a particular absorption line of acetylene at 1531.53 nm. The measured results (the crosses) are in close agreement with the theoretical prediction (the solid line) from an equivalent system model of twice the length (i.e., 20 cm) with two ends opened for

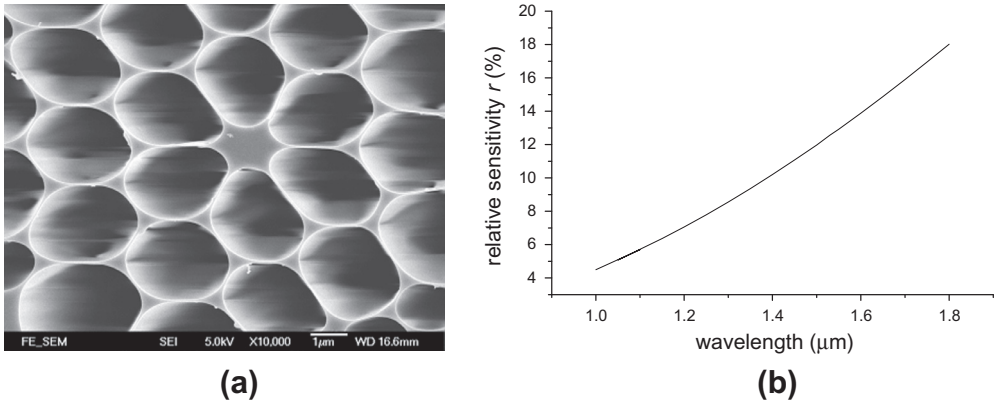

Fig. 5. (a) Cross-section of the highly non-linear fiber from Crystal Fiber A/S. Diameter of the central silica region is ~1.7 μm, and the pitch and the diameter of the cladding holes are respectively Λ = ~3.24 μm and d = ~3 μm. (b) The relative sensitivity r as a function of wavelength. Reprinted from [31], Copyright (2003), with permission from OSA.

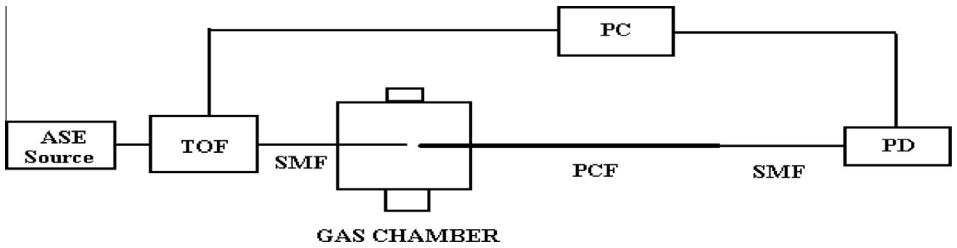

Fig. 6. The first demonstration of gas detection with PCF. TOF: Tunable Optical Filter; PD: Photo-detector; PC: Personal Computer. Reprinted from [31], Copyright (2003), with permission from OSA.

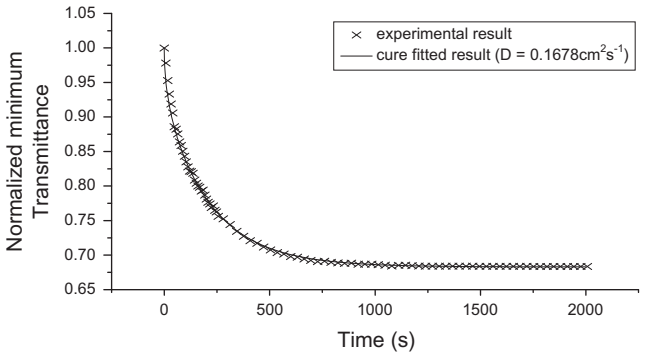

Fig. 7. Measured normalized minimum transmittance at 1531.53 nm as function of time. Reprinted from [31], Copyright (2003), with permission from OSA.

diffusion. The relative sensitivity was determined from the minimum transmittance to be ~13.6%.

Further theoretical modeling of the gas diffusion dynamics showed that the response time, defined as the time taken for the average concentration of detected gas (C_2H_2) in the air-columns over the entire sensing length reaches 90% of the surrounding gas concentration is found to be 63 s for a 7 cm long PCF. For gas sensing application that requires response time of ~1 min, the length of the sensing PCF should be limited to less than 7 cm, assuming both ends are open for diffusion.

From above discussion, it becomes clear that by use of a long length of IG-PCF, high sensitivity gas detection may be achieved. However, the long response time needed for gas to diffuse into the holes from the ends of PCF is an issue that needs to be addressed. The introduction of side openings by for example etching into the innermost holes to get access to the EW from aside was proposed [31], however, it is challenging to implement it in practice considering the complex microstructured holey cladding structure of the fiber. The other issue is the low-loss connection between a small-core IG-PCF and a standard SMF. Since the effective mode field diameters of the two types of fibers are significantly dif-

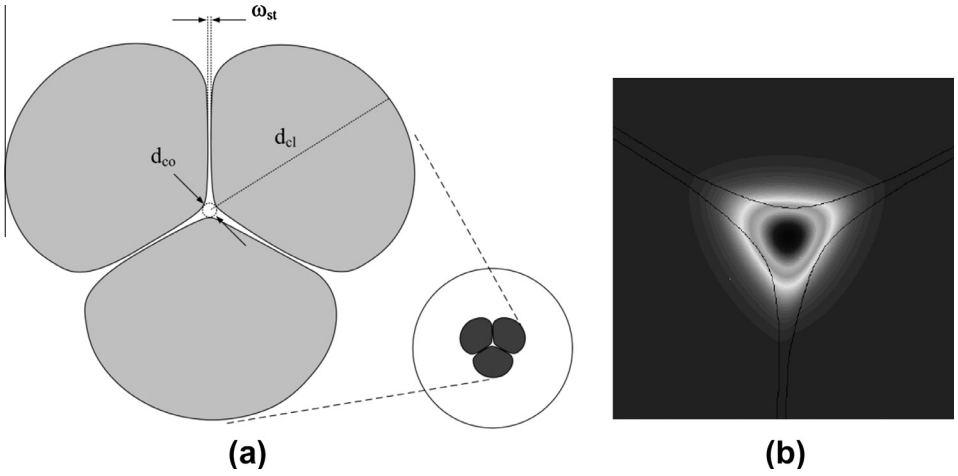

Fig. 8. (a) Sketch of a SCF reported by Selleri et al. [68]. d_{co}, d_{cl} and ω_{st} represent respectively the core diameter, cladding hole diameter, and struts width; (b) Distribution of the fundamental mode (magnetic field) for the SCF with d_{co} = 1.17 μm, d_{cl} = 24.5 μm and ω_{st} = 0.19 μm at λ = 1550 nm. Reprinted from [68], Copyright (2009), with permission from SPIE.

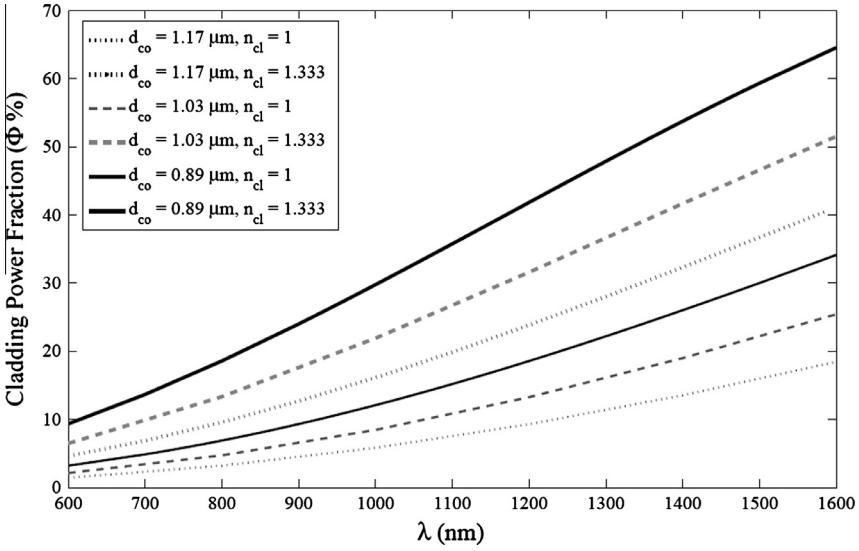

Fig. 9. Fraction of EW of the fundamental mode for SCFs with different core diameters when holes are filled with air (n_{cl} = 1) or water (n_{cl} = 1.33). Reprinted from [68], Copyright (2009), with permission from SPIE.

ferent, the direct splicing loss can be very large. The loss may be reduced to an acceptable level by use of an intermediate fiber [65].

SCFs have a wavelength or sub-wavelength scale solid core supported by few thin struts connected to the outer cladding [66,67]. Fig. 8(a) and (b) show respectively the cross section of a particular SCF with 3 struts and the fundamental mode distribution of magnetic field at the wavelength of 1550 nm [68]. The very small solid core and the large index contrast results in tight confinement of light and strong evanescent field extending into surrounding air-holes. Fig. 9 shows the relationship between wavelength and power fraction of fundamental mode in the air-holes with different core diameters. The holes are filled respectively with air (refractive index $n_{cl} = 1$) and water ($n_{cl} = 1.33$). The power fraction of evanescent field increases with reducing core diameter, and a power fraction up to 30% in air can be achieved with a SCF with core diameter of 0.89 μm at $\lambda = 1550$ nm. Investigations on the SCFs with similar structures have been carried out by Webb et al. [35], Cordeiro et al. [69] and Monro et al. [67,70], respectively.

Similar to IG-PCF, gas diffusion rate limits the response time of the SCF-based sensors. Webb et al. carried out experimental tests with a 1 m long SCF with a core diameter = 1.2 μm, hole diameter = 8 μm and strut thickness = 0.2 μm [35], and it took about 7 h to fill the SCF with 100% C_2H_2 by free diffusion. However, since SCFs have only a few larger size air-holes and hence it is relatively easier (compared with IG-PCFs) to fabricate side-openings to get access to the evanescent field. van Brakel et al. demonstrated the fabrication of a micro-channel by use of femtosecond infrared laser by which one third of the evanescent field of the fiber can be accessed and the loss introduced was found to be 0.5 dB [71]. For the structure shown in Fig. 8a, three micro-channels drilled into the three hole-columns would be sufficient to make a full access of the entire evanescent field.

Alternatively, SCFs with exposed-core may be made directly during fiber-drawing process. Cox et al. [72] reported a polymethyl methacrylate (PMMA) SCF fabricated by drilling lateral holes into the preform in addition to the standard drawing process by which a slot was created along the length of the fiber and one out of three cladding hole-columns was open to the surrounding environment. Warren-Smith et al. [73] reported the fabrication of exposed-core SCFs with lead-silicate glass, which is directly drawn from a slotted wagon wheel structured preform. The average loss of these exposed-core SCFs over the 400–1600 nm wavelength range is from 2.2 to 4.1 dB/m, depending on the thicknesses of the struts. More recently, a low loss exposed-core silica SCF was reported by Kostecki et al. [74]. The fiber was directly drawn from a slotted perform and the cross-section is shown in Fig. 10.

Similar to the IG-PCF, a problem associated with the use of SCF for gas detection is the efficient coupling of light from source to SCF and between a SCF and a standard SMF. Chen et al. demonstrated direct-coupling of vertical-cavity surface-emitting lasers (VCSELs) of 763 nm, 1674 nm and 2004 nm to a SCF by which in-fiber O_2, CH_4 and CO_2 sensing was performed [75]. The coupling efficiencies for the 763 nm and 1674 nm VCSELs are 13% and 15% respectively while the value for 2004 nm laser was not provided. Dong et al. demonstrated fusion splicing of a SCF with a core diameter of ~1.27 μm to Hi1060 via an intermediate fiber (Nufern, NA = 0.35, diameter = 2.1 μm), and the total loss for the two splices was measured to be ~0.8 dB [76].

In summary, small-core IG-PCF and SCFs have large percentage of optical power located within air-holes and may be good platform to study gas-light interaction via evanescent field. The state of the art IG-PCFs and SCFs have a sufficiently low attenuation, which allows the use of long (tens of meters) such fibers for high sensitivity gas detection. Compared with IG-PCF, it is easier to fabricate side-openings on a SCF or to expose the core of a SCF, since it has only one ring of air-holes surrounding the core. SCFs are then better candidate for high sensitivity gas detection with fast response. In addition, both IG-PCF and SCFs have broad low-loss transmission windows and it is possible to use them for the detection of multiple gas species, assuming they have absorption lines within the transmission band of the fibers.

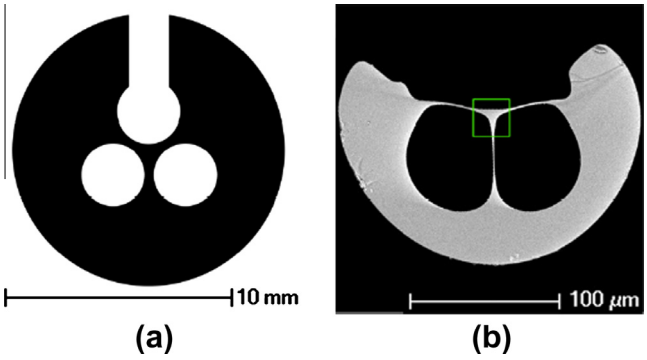

Fig. 10. Exposed-core silica fiber drawn from a slotted preform: (a) cross section of the preform and (b) SEM image of the fiber. Reprinted from [74], Copyright (2012), with permission from OSA.

2.3. Gas detection with hollow-core optical fibers

Hollow-core photonic bandgap fibers (HC-PBGFs) also belong to the family of microstructured fibers [77]. Unlike IG-PCFs and SCFs, HC-PBGFs guide light through photonic bandgap effect. Since the its first demonstration in 1999 [78], significant progress has been made in the design and fabrication air/silica HC-PBGFs. The

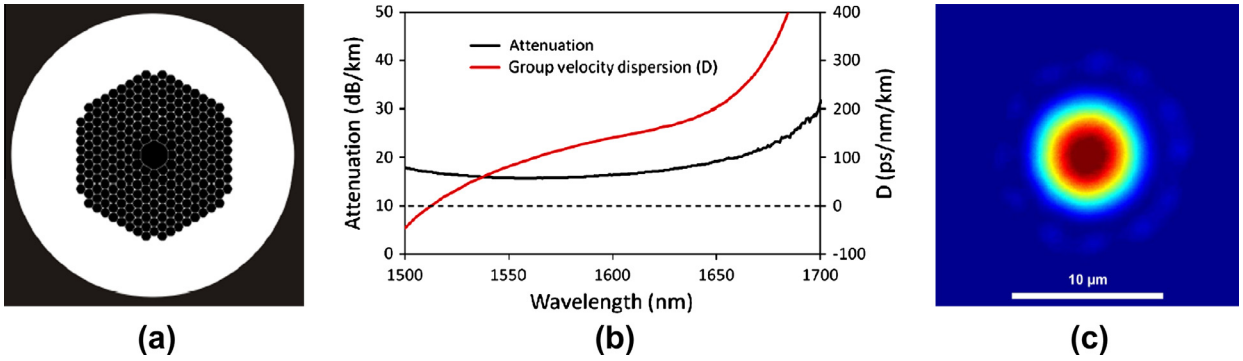

Fig. 11. (a) Schematic cross section of a commercial HC-PBGF (NTK Photonics A/S, HC-1550-02), (b) Transmission characteristic of the fiber, and (c) Typical near field intensity profile of the fundamental mode. Reprinted from [82] with permission from NKT Photonics A/S.

minimum fiber loss has been reduced down to 13 dB/km at 1500 nm in 2003 [79] and 1.2 dB/km at 1620 nm in 2005 [80].

Compared with IG-PCFs and SCFs, the transmission window of a HC-PBGF is much narrower and on the order of a few hundreds of nanometers. Fig. 11(a) shows the cross section of a commercial HC-PBGF with a seven-unit-cell air core (NKT HC-1550-02 fiber). This fiber has a transmission window from 1490 to 1680 nm (Fig. 11(b)), within which several guided modes are supported. The intensity distribution of the fundamental mode is shown in Fig. 11(c). However, HC-PBGFs with different transmission bands may be fabricated by varying the diameter and pitch of the air-holes. HC-PBGFs with transmission windows from 440 nm to 2 μm are now commercially available [81].

HC-PBGFs allow the confinement of an optical mode and gas phase materials simultaneously within the hollow-core. This provides an excellent platform for strong light/gas interaction inside the fiber core over a long distance. Long HC-PBGFs can be coiled to very small diameters (e.g., 1 cm) without introducing significant loss, allowing highly sensitive and compact "point" sensors to be developed. A typical HC-PBGF designed to operate at 1550 nm have a transmission window of ~200 nm, covering the absorption bands of many important gases such as CO, CO_2, NH_3, H_2S, C_2H_2 and CH_4.

The possibility of using HC-PBGFs for gas sensing was raised by Cregan et al. as early as the first air/silica HC-PBGFs was demonstrated [78]. In 2004, Hoo et al. reported online the results of the experimental investigation on gas diffusion measurement with HC-PBGF [32]. After a short while, Ritari et al. reported the demonstration of high sensitivity gas sensing using HC-PBGFs with transmission windows cnetred at 1300 and 1500 nm respectively with which detection of C_2H_2, HCN, CH_4 and NH_3 gas was performed [33]. They have also investigated the dynamics of gas filling and evacuation processes under vacuum conditions down to 10 mBar, and concluded that the use of higher pressure results in a shorter filling time and a longer evacuation time. A more detail analysis on the dynamics of gas flow in HC-PBGFs has been carried out by Henningsen et al. in 2008 [83].

Similar to IG-PCF and SCF based sensors, the slow response due to time taken for gas filling and venting is an obstacle for developing practical HC-PBGF gas sensors. Different approaches for improving the response time of the HC-PBGF sensors have been reported. Wynne et al. reported a pressure-driven gas-filling method [84] by which the filling times have been significantly enhanced by a pressure differential applied between the two ends of the sensing fiber. However, this method is restrictive for a compact fashion; and more importantly it is not suitable for real-time gas sensing applications where no pressure differential is guaranteed. Methane sensors using multiple segments of HC-PBGF with coupling gaps has been reported by Parry et al. [85] and Carvalho et al. [86] respectively. Fig. 12 illustrates an assembly of a multi-segment HC-PBGF gas sensor and different approaches for butt-coupling. However, the coupling loss between the segments may limit the number of segments. In addition, alignment between the fiber segments may affect the compactness and stability of the sensor.

In 2005, Lehmann et al. [87] reported fabrication of microchannels into the core of HC-PBGFs by using a 193 nm ArF laser with a repetition rate of 50 Hz (Fig. 13(a)). Cordeiro et al. [88] demonstrated a local-heating/pressure-assisted method for formation of a side hole (side opening) through the wall of a HC-PBGF. The method is based on increasing the pressure inside the air holes of MOF while local heat is applied at the desired position of the side-opening by using a standard fusion splicer. The heated fiber segment expanded and was laterally torn, thus a side-opening is formed (Fig. 13(b)). Besides, a focused ion beam (FIB) milling technique may be implemented for introducing side-openings. This technique has been used for cutting [89] and creating a small channel [90] at the end of HC-PBGF (Fig. 13(c)).

Femtosecond (*fs*) laser micromachining [91] is an alternative technique for fabricating microchannels on SMFs and MOFs. Lai et al. demonstrated the fabrication of a microchannel of 4 μm in diameter in a conventional SMF by means of *fs* laser processing and chemical etching [92]. Hensley et al. [93] reported the drilling of six evenly spaced holes over a 2 mm section of a 33-cm long HC-PBGF. Index-matching fluid with $n = 1.45$ was used to circumvent the fiber and continuously pumped into the core and cladding holes in order to keep the tight focus of *fs*-laser pulses into the cylindrical fiber. Keep circulating of fluid would also help in removing the debris inside the fiber produced during the laser drilling process. With this approach, microchannels with a diameter of 1.5 μm on the surface of the fiber were fabricated. However, the loss induced by each channel was estimated to be 0.35 dB. The ends of the HC-PBGF were fusion spliced to two sections of SMF to form an all-fiber variable-pressure gas cell. van Brakel et al.

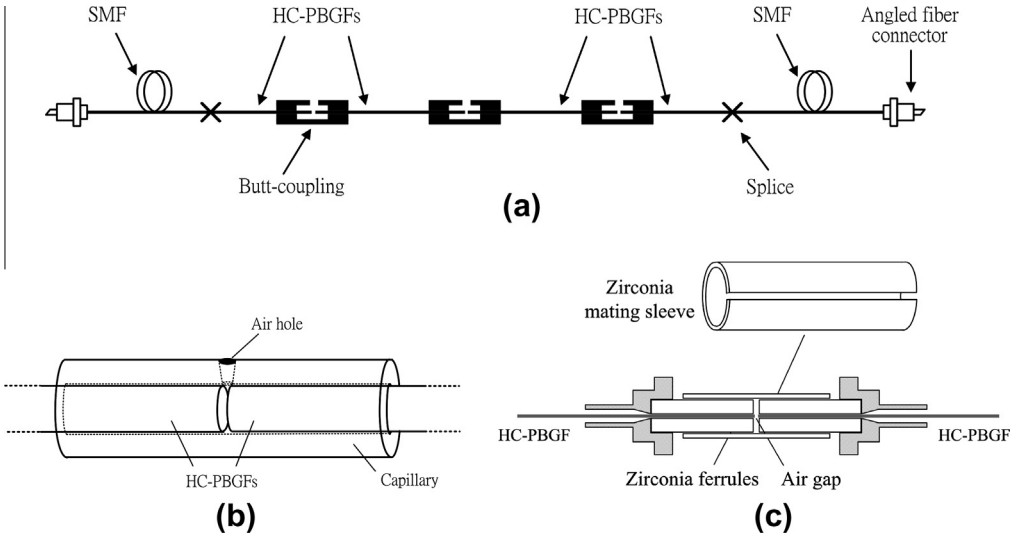

Fig. 12. (a) Assembly of a multi-segment HC-PBGF gas sensor; (b) HC-PBGFs butt-coupling within a glass capillary tube on which an air-hole is introduced for gas filling [85]; (c) Standard zirconia ferrules connected with a standard zirconia mating sleeve for HC-PBGFs butt-coupling [86] where gases can diffuse into the air-core through the slit of the mating sleeve.

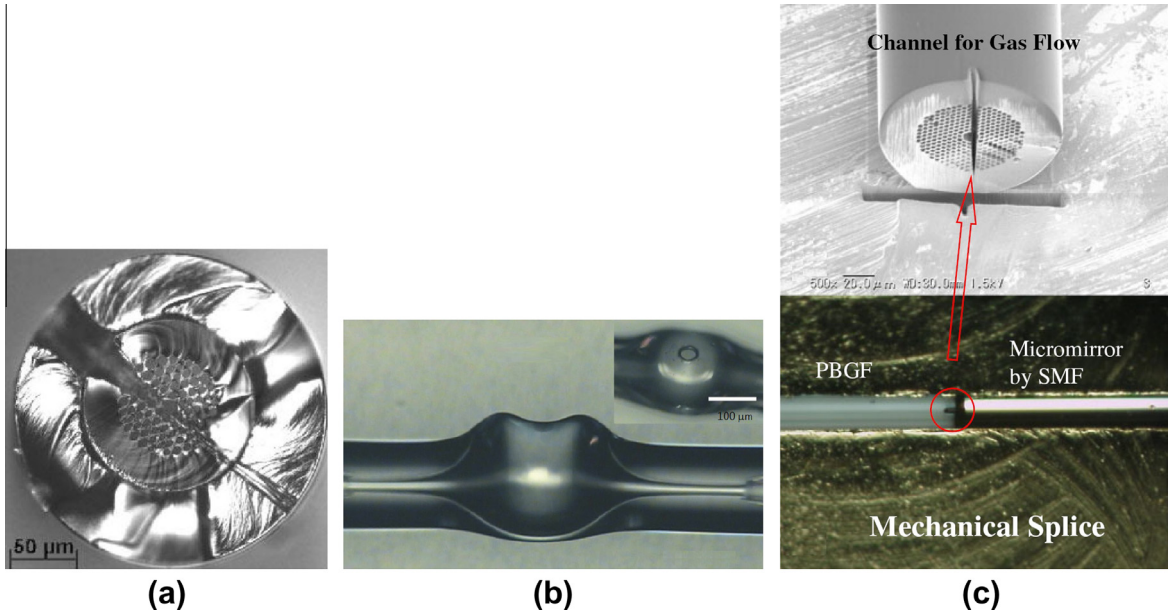

Fig. 13. (a) Cross section of HC-PBGF with a microchannel created by ArF laser. Reprinted from [87], Copyright (2005), with permission from SPIE. (b) Sidehole created by local-heating/pressure-assisted method. Reprinted from [88], Copyright (2006), with permission from OSA. (c) A microchannel at the end of HC-PBGF fabricated by FIB milling. Reprinted from [90], Copyright (2011), with permission from Japanese Journal of Applied Physics.

[71] fabricated microchannels in both acrylate-coated and uncoated HC-PBGFs. The success in fabrication of microchannels in the coated MOF is important for preserving the mechanical strength of the fiber which is an advantage for developing practical sensors. Gas cells of 2-m long with either 1 or 2 microchannels have been constructed and used in out-diffusion experiments. As shown in Fig. 14, the rate of out-diffusion was significantly accelerated after the introduction of the second microchannel.

HC-PBGFs gas sensor with high detection sensitivity and fast response may be realized by fabricating a number of side-openings or microchannels along a long length of the fiber. The major premise is achieving a low drilling-induced loss which has been demonstrated by Jin et al. [94]. Fig. 15 shows a typical *fs*-laser setup for microchannel fabrication on HC-PBGF. The fiber is mounted on a computer-controlled, three-axis translation stage. The femtosecond laser is first focused and aligned on the fiber surface, and then the focus point is moved towards the fiber core. This process is repeated for several times and thus a micro-channel from fiber surface to fiber core is created. Fig. 16(a) and (b) shows the side-view and cross-section of a microchannel created on the HC-1550-02 fiber. The average loss from 1500 to 1650 nm for a 30 cm long HC-PBGF with 20 evenly distributed micro-channels was measured to be ~1 dB (Fig. 16(c)), corresponding to a loss of ~0.05 dB per channel.

With the *fs*-laser micromachining technique, a fast response HC-PBGF methane sensor with multiple micro-channels has been demonstrated by Hoo et al. in 2010 [95]. The sensing fiber was a piece of 7 cm-long HC-1550-02 PBGF with 7 microchannels, each separated by ~1 cm. A diffusion limited response time of ~3 s and a sensitivity of ~647 ppm for methane gas have been achieved. Fig. 17(a) shows the setup for the gas detection experiments, and fig. 17(b) is the measured response of during an out-diffusion process with the cell initially filled with ~ 5% methane at ambient pressure.

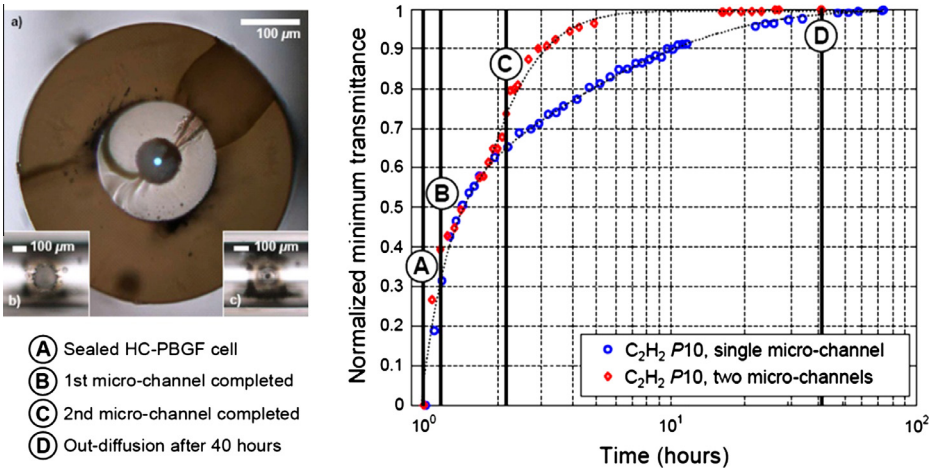

Fig. 14. (Left) Cross section of acrylate-coated HC-PBGF with a microchannel; (Right) Results of the out-diffusion experiments which showed the diffusion rate was accelerated after the 2nd micro-channel was introduced (just before C). Reprinted from [71], Copyright (2007), with permission from OSA.

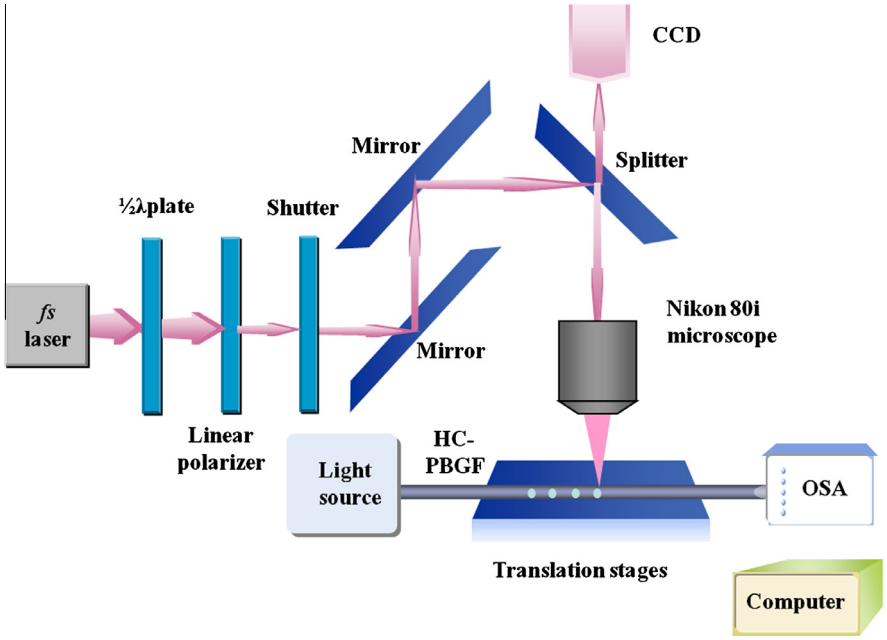

Fig. 15. The *fs* laser system for fabricating microchannels in a HC-PBGF.

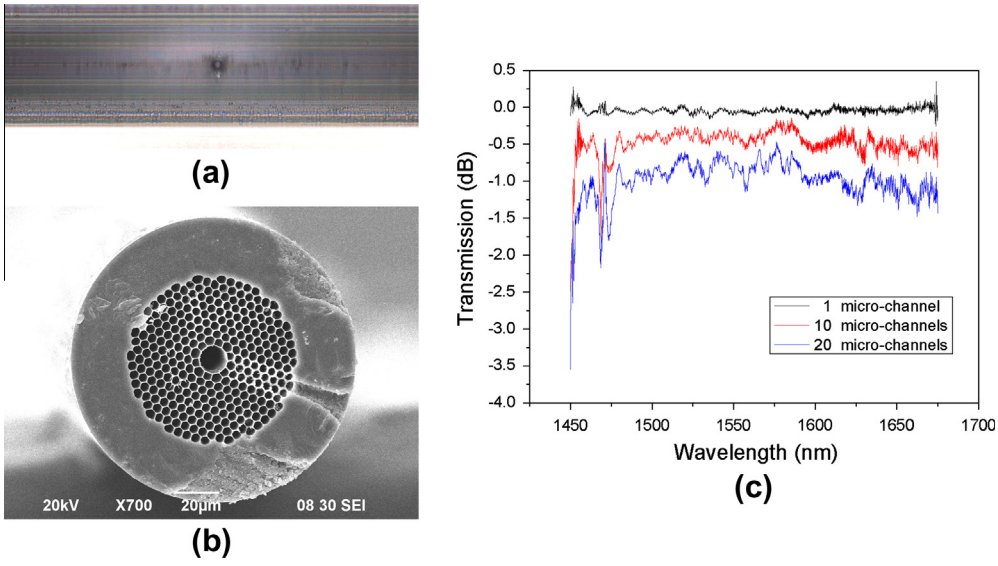

Fig. 16. (a) Side-view and (b) cross-section of a microchannel fabricated on the HC-1550-02 fiber. (c) Loss spectrum of a 30 cm long HC-1550-02 fiber with 1 micro-channel, and 10 and 20 microchannels evenly distributed along the fiber.

3. Photoacoustic spectroscopic gas sensing with optical fibers

3.1. Principle of photoacoustic spectroscopy

Photoacoustic spectroscopy (PAS) is another important technique that is widely used for trace gas detection [96–98]. The basic operating principle of a PAS based gas sensor is illustrated in Fig. 18. A laser beam with its intensity or wavelength perioedically modulated is delivered to a gas cell within which light energy is absorbed by gas molecules, and an acoustic pressure wave is then generated via the photoacoustic (PA) effect. The acoustic wave is then detected by a sensitive acoustic tranducer or microphone and further data processing is employed to recover the gas concentration. A detailed description of the PA effect can be found in [99].

As the detection object in PAS is acoustic pressure instead of optical intensity, gas detection based on PAS would have the following characteristics or advantages:

(1) No background signal. The PA signal is proportional to light absorption by target gas, there is no acoustic signal without light absorption.
(2) For a specific microphone, the acoustic signal is not significantly affected by the optical path length, as long as the absorption region covers the size of the microphone. This means that extremely compact sensors could be developed with good sensitivity.

In addition, by use of a multi-pass gas cell to increase the light energy absorbed by the gas molecules and/or an acoustic resonator

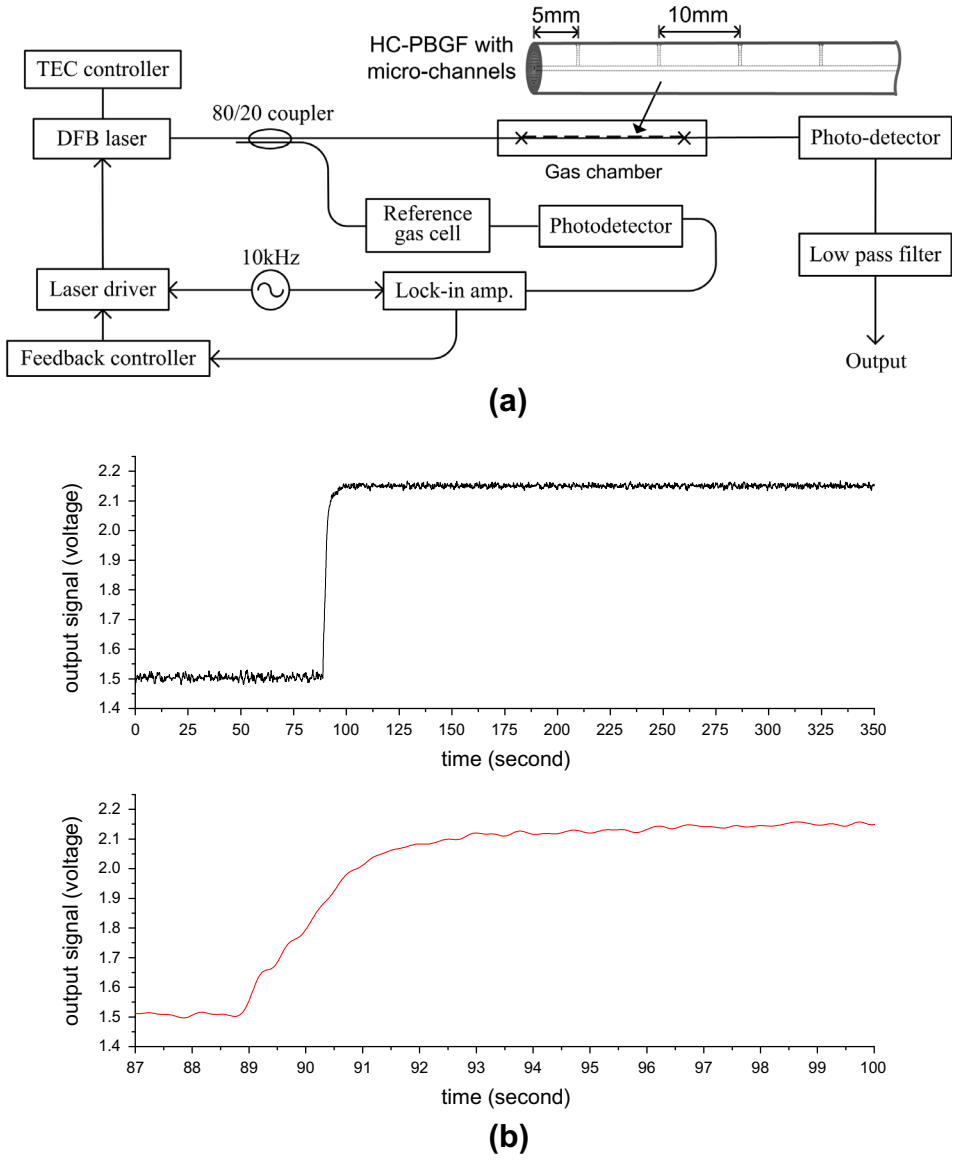

Fig. 17. (a) Experimental setup for gas detection with HC-PBGF. (b) Output signal measured during methane out-diffusion as a function of time. The gas cell is initially filled with ~5% methane and sealed and then opened for out-diffusion at ~89 s. The measurement was conducted at the methane absorption line at 1665.48 nm [95].

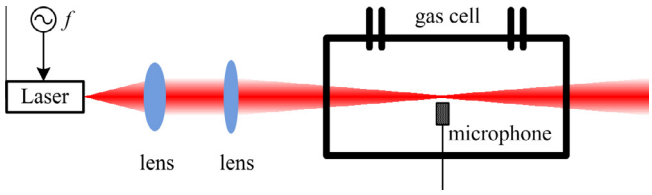

Fig. 18. Principle of PAS based gas detection.

to enhance the accumulation of acoustic energy in the cell, the detection sensitivity may be further improved.

3.2. PA excitation with optical fibers

In early PAS systems, laser beam is coupled into the PA cell via free space optics with bulky collimating/focusing lenses (Fig. 18). Optical beam should be carefully collimated and focused to a specific region for efficient generation and detection of acoustic wave. This is especially the case when an acoustic resonator is used to enhance the acoustic detection and precise assembly of the setup is then required and the system is sometimes complicated and cumbersome.

The use of fiber pigtailed collimator lens (Fig. 19) ease the alignment and at the same time allows the delivery of excitation light through the optical fiber. This allows the light source be located remotely from the senor head and in a well controlled environment.

Taking advantage of the EW of a tapered optical microfiber, we demonstrated that the acoustic wave can be generated by the EW of a microfiber as shown in Fig. 20(a), which avoids the use of complicated collimating/focusing optics [100]. With a quartz tuning fork as the acoustic probe, we tested several fiber tapers with different diameters (Fig. 20(b)) and the normalized noise equivalent absorption coefficient of 1.96×10^{-6} cm^{-1} W/Hz$^{1/2}$ was achieved with a fiber taper of a diameter of 1.1 μm. By reducing the fiber diameter, the power percentage in the evanescent field could be further enhanced, which promises a gas detection sensitivity comparable to that of a conventional open path PAS sensor. In PAS, the generated signal is not determined by the absorption path length

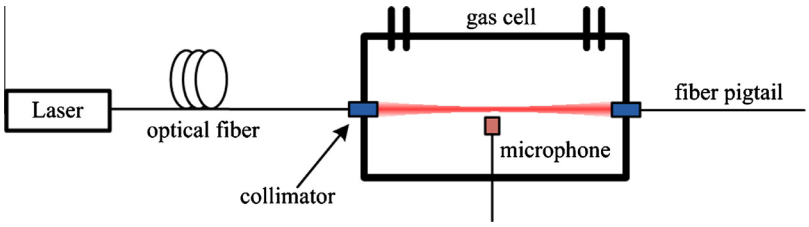

Fig. 19. Remote delivery of excitation light to a PA cell via optical fiber with a collimator lens at its end.

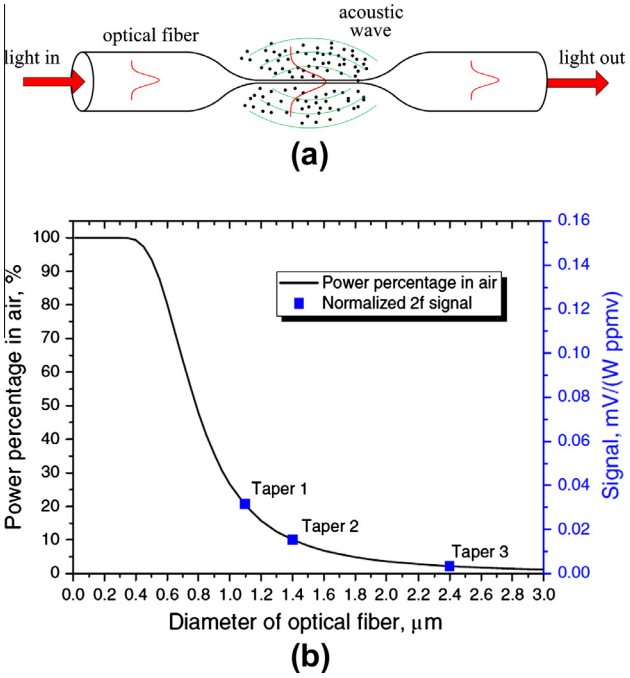

Fig. 20. (a) Schematic of PA excitation via evanescent field of a tapered optical microfiber. Red profiles illustrate the variation of the optical mode field along the fiber, black dots indicate gas molecules and green curves represent acoustic wave generated via PA effect; (b) Measured second harmonic PA signal for three different fiber tapers and the calculated power percentage in air as function of taper waist diameter. Reprinted from [100], Copyright (2012), with permission from OSA. (For interpretation of the references to color in this figure legend, the reader is referred to the web version of this article.)

but the localized acoustic pressure amplitude and the detection sensitivity of the microphone. Therefore, a micro/nano fiber with a length of slightly larger than the size of the microphone would be sufficient, avoiding the use of a long fiber taper and the problems associated with it.

Recently, we fabricated in-fiber photonic microcells by tapering and locally inflating a section of a commercial IG-PCF [101]. The microcell is basically a microfiber suspended within an inflated capsule and is more robust compared with a bare micro/nano fiber. By introducing side openings from aside of the capsule, microchannels for gas circulation can be created. Such a microcell may be used to excite acoustic wave inside the capsule via PA effect.

We also demonstrated the excitation of PA pressure wave inside a miniature Fabry–Perot cavity [41]. The schematic of which is shown in Fig. 21. Gas diffuses into the cavity from a small side-opening and interacts with the wavelength modulated laser beam to generate periodic acoustic pressure wave. The pressure wave causes deflection of the thin diaphragm, which is detected by another probe laser through the same Fabry–Perot Interferometer (FPI). The details of the system are described in Section 3.4 and in Fig. 26.

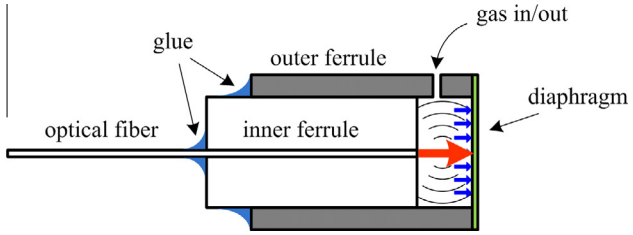

Fig. 21. Schematic of PA excitation in a fiber-tip Fabry–Perot cavity. Red arrow presents the optical beam for PA excitation, blue arrows indicate the acoustic pressure impinging the diaphragm. Reprinted from [41], Copyright (2013), with permission from OSA. (For interpretation of the references to color in this figure legend, the reader is referred to the web version of this article.)

3.3. Fiber-optic microphone for PAS

The general role of a microphone is to transfer the acoustic pressure wave into a specific sort of vibration and measure its amplitude via electrical or optical means. The sensitivity of the microphone would ultimately determine the capability of the PAS based sensing system.

Most of the PA systems reported so far use electric capacitive microphones [102–104], which transforms the acoustically induced membrane vibration into an electric signal. An alternative is to use a piezoelectric transducer such as a quartz tuning fork [105–107]. In this case, the acoustic energy is accumulated in the resonant piezoelectric device, and the vibration of the piezoelectric device is converted into electric signal via piezoelectric effect. The detection sensitivities of these two configurations are showed to be extremely high and the sensor sizes are also very compact. However, the electric nature of the microphone limits their applications in circumstances with electromagnetic interference, as well as remote detection capability.

Attempts have been made to develop optical and fiber-optic microphones for PA detection. de Paula et al. reported an optical microphone made with a thin reflective pellicle bound on the edge of a PA cell [108]. The variation of the cell walls causes the pellicle be deflected and the position of the pellicle can then be measured by a probing optical beam. By selecting alternative pellicle material and properly tailoring its dimensions [109,110], they improved the sensitivity of their sensors by 4–5 orders of magnitude. Another example of optical microphone is based on a micro-cantilever as shown in Fig. 22(a) [39,111,112]. A micro-cantilever fabricated from a silicon base is placed on the wall of the PA cell at the maximum acoustic pressure point to detect the PA pressure wave. The deflection of it is measured by an external Michelson Interferometer (MI). This configuration provides the highest gas detection sensitivity with laser-based PAS to date [112]. However, this setup is complicated and the system assembly is required to be precise. Recently, Kohring et al. demonstrated a novel optical microphone by combining the high sensitivity of a quartz tuning fork and the advantages of optical interferometric measurement as shown in

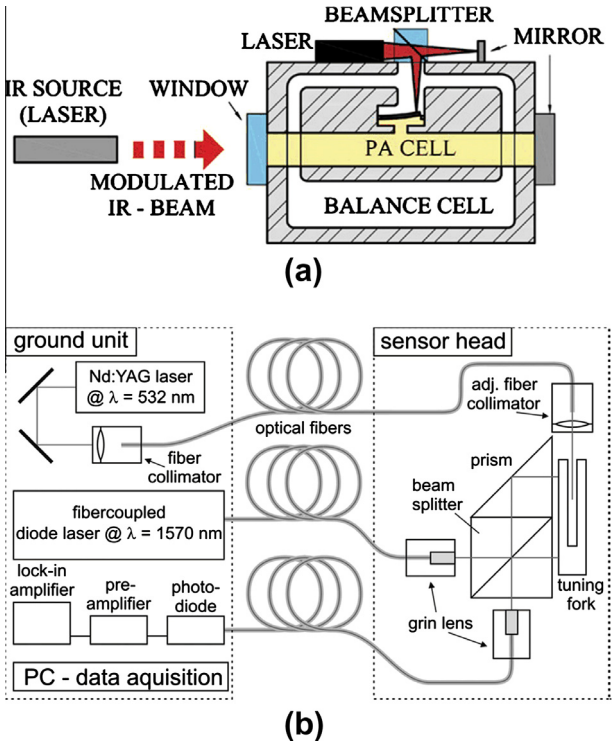

Fig. 22. Schematics of PAS systems with different optical microphones. (a) Micro-cantilever. Reprinted from [112], Copyright (2008), with permission from Elsevier. (b) A tuning fork. Reprinted from [114], Copyright (2012), with permission from IEEE.

Fig. 22(b) [113,114]. They also used optical fibers to deliver light to and collect light back from the PA cell.

The first attempt to use optical fiber to detect PA pressure wave was reported by Leslie et al. in 1981 [115]. In their system, a 9.2-meter-length optical fiber was wound around a 2.45 cm, mylar-coated mandrel as the microphone. The PA pressure wave modulates the phase of light signal in the sensing arm, which was measured by a Mach–Zehnder interferometer (MZI) as shown in Fig. 23. In 1995, Breguet et al. presented an optical-fiber microphone constructed by winding and gluing a fiber coil on a thin plate of the gas cell wall [116]. The length of the fiber coil is modulated via the deformation of the cell wall due to the first longitudinal acoustic mode applied on the plate. Michelson and Sagnac interferometers were employed to detect the optical phase change. With this configuration, gas (ethanol and ozone) detection limit down to ~ppb level was achieved with a 0.6-W CO_2 laser source. It has been reported that an optical fiber coil can also be used as a microphone by monitoring its transmission loss due to micro-bending resulted from absorption-induced acoustic field [117].

Fiber-tip sensors are another type of microphone that may be used for PA detection [40,41,118]. This type of microphone is typically based on a fiber-tip FPI. Because of its compact size, this type of fiber probes would be particular useful for space-limited applications. In 1998, Beard et al. demonstrated a fiber-optic PA probe for photoacoustic and photothermal measurements in liquid absorber [118]. In their experiment, a sensitive layer of film was attached to the fiber tip to form a FPI (Fig. 24(a)). When the fiber-tip probe is subjected to a PA induced thermal or acoustic field, the thickness of the film changes, which causes the optical phase modulation of FPI to give out a modulated light intensity. The optical intensity signal was demodulated to show a linear relationship with the absorbance in the target. Recently, a fiber-tip microphone with a polymer diaphragm based extrinsic FPI (EFPI) was reported [40,41]. The FPI is formed by the endface of the optical fiber and the inner surface of the polymer diaphragm as shown in Fig. 24(b). The deformation of the diaphragm resulted from the PA pressure wave changes the Fabry–Perot cavity length, which can be demodulated by monitoring the reflected light intensity variation when the operation point is tuned or stabilized to a linear slope point of the interference fringe. The sensitivity of this method is determined by the dimension (diameter and thickness) and the mechanic properties of the diaphragm. Recently, fiber-tip Fabry–Perot pressure sensors with extremely thin photonic crystal [119], silver [120,121], and graphene diaphragms [122,123] are reported, these sensors would have improved sensitivity and a smaller size, and are ideally suited for PAS based gas sensors.

A key issue for the interferometric detection of acoustic wave is the signal demodulation. In most of the reported systems, a single wavelength laser tuned to the quadrature point of the interference fringe is adopted to acquire the signal amplitude. However, the fluctuation of the operation point due to various factors, such as temperature variation and laser wavelength drift, would affect the detected signal. Therefore, the stabilization of the operation point must be deal with in real time applications.

The performance of some PAS systems with optical or fiber-optic microphones is summarized in Table 2. The performances of fiber-optic microphone-based systems are already comparable to their electrical counterparts. However, the excitation and detection

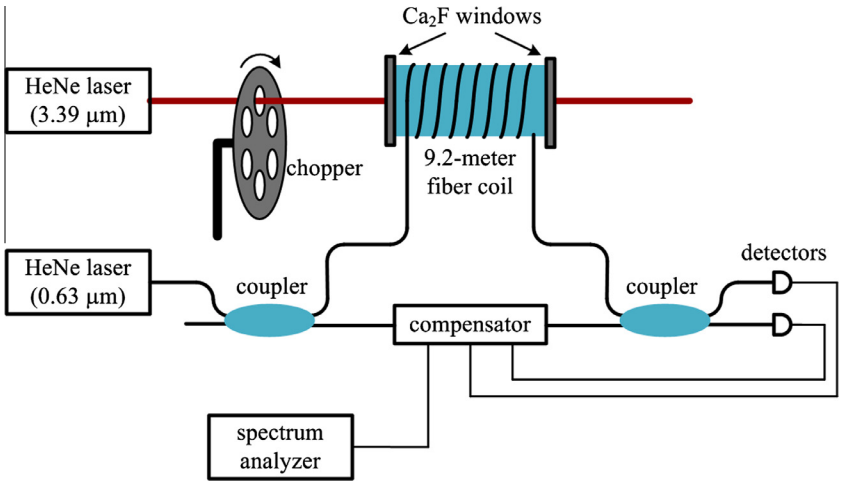

Fig. 23. Configuration of a fiber-optic microphone for PAS gas detection [115].

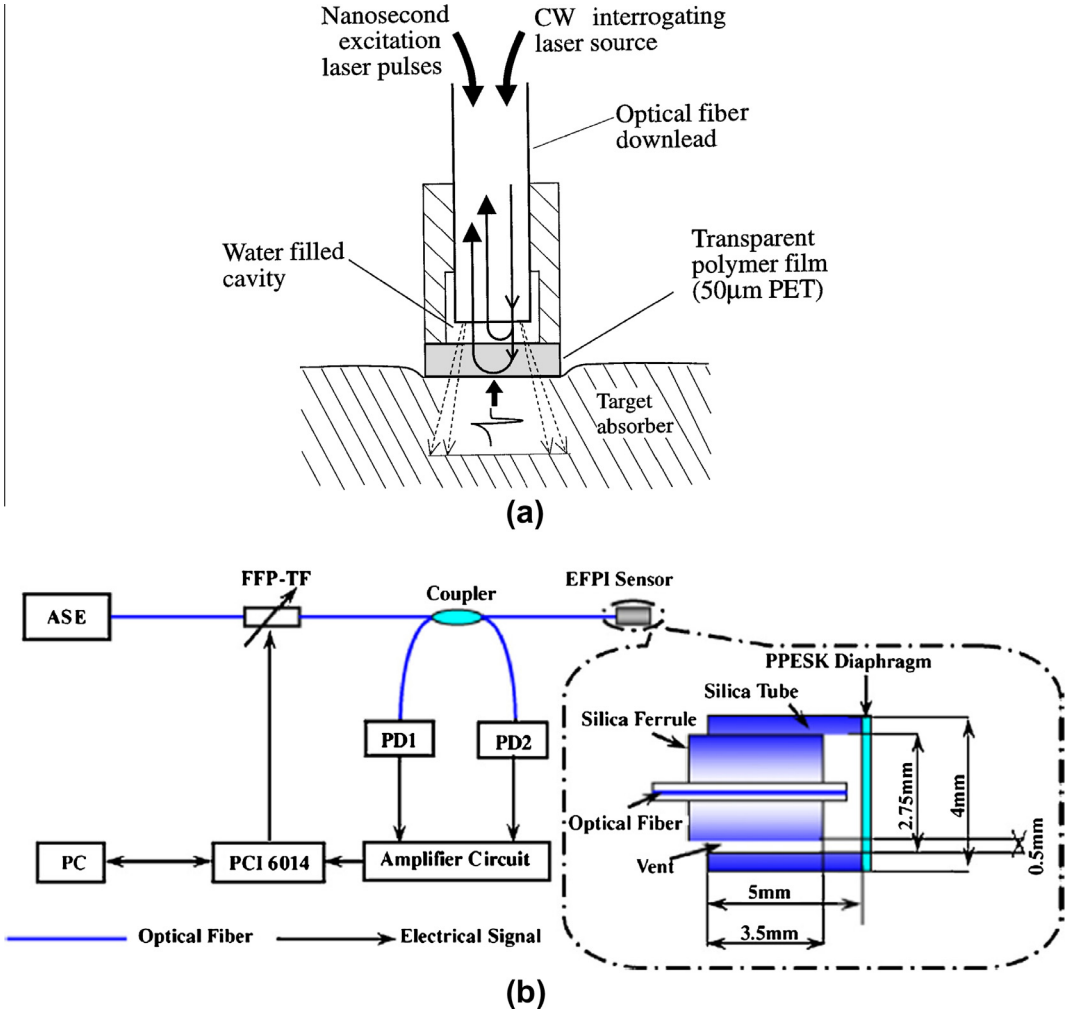

Fig. 24. Schematic diagrams of fiber-optic acoustic probes. (a) Two surfaces of the polymer film forms a FPI. Reprinted from [118], Copyright (1998), with permission from OSA. (b) Fiber endface and polymer diaphragm's inner surface forms a FPI. Reprinted from [40], Copyright (2011), with permission from Elsevier.

Table 2
Characteristics of some optical and fiber-optic microphones.

Type	$\alpha_{min} \cdot P$ (cm^{-1} W)[a]	Advantages	Main problems
Cantilever with external MI [124]	1.08×10^{-10}	High sensitivity	Difficult to assemble, not-applicable to remote sensing
Fiber coil with MZI [116]	2.62×10^{-9}	Remote detection capability	Relatively large sensor size
Fiber-tip probe with FPI [40]	4.86×10^{-10}	Compact size, high sensitivity, remote detection capability	Complicated fabrication process

[a] Minimum detectable absorption coefficient normalized by excitation power.

of PA signal in fiber-optic format would allow the realization of remote detection and multiplexed multi-point detection within a fiber optic network, taking advantages of large bandwidth and low loss characteristics of optical fibers.

3.4. All-fiber PAS-based gas sensors

With fiber-optic delivery of the excitation light and probing of the PA pressure wave, all-fiber PAS based gas sensors may be developed. Fig. 25 shows an all-optical PA system reported by Wang et al. [40]. With a polymer-diaphragm-based EFPI (Fig. 24) operating at the quadrature point of interferometric fringe as the acoustic probe, they achieved a minimum detectable acetylene concentration level of 1.56 ppb by using a fiber laser with wavelength around 1530.37 nm and amplified power of 500 mW as the excitation laser.

We recently demonstrated a miniature all-fiber PAS gas sensor as shown in Fig. 26 [41]. The sensor head comprises of a fiber-tip FPI with a thin polymer diaphragm (Fig. 21), which acts as a PA cell for light-gas interaction, as well as an acoustic probe. An excitation laser with wavelength $\lambda_e = 1.53$ μm and optical power of 8 mW is delivered to the Fabry–Perot cavity to excite PA pressure wave, and another probe laser with wavelength tuned to the linear region of the FPI interference fringe ($\lambda_p = 1556.1$ nm) and with a power of 4 mW is coupled to the same FPI to measure the cavity length variation induced by the acoustic pressure wave. With this setup, a minimum detectable acetylene concentration level of 4.3 ppm was achieved corresponding to a minimum absorption coefficient normalized to optical power of $\alpha_{min} \cdot P = 1.07 \times 10^{-8}$ cm^{-1} W.

4. Networked and distributed fiber optic gas sensors

4.1. Multiplexed multipoint gas sensor network

An effect means for cost reduction is through multiplexing in which expensive components such as source and transmission

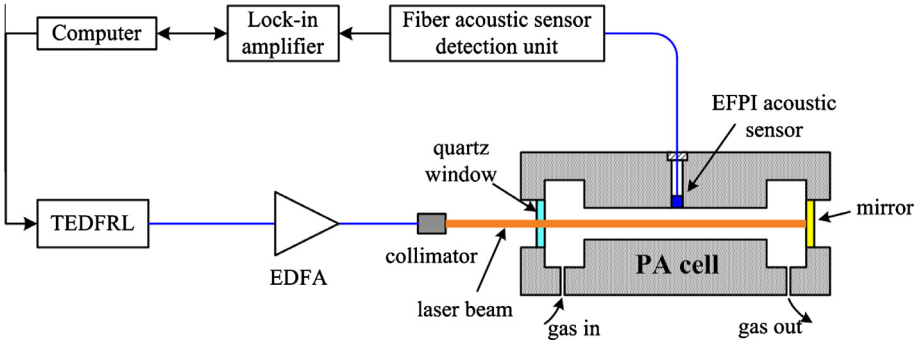

Fig. 25. An all-optical PAS gas sensor system [40]. TEDFRL: tunable erbium-doped fiber ring laser, EDFA: erbium-doped fiber amplifier.

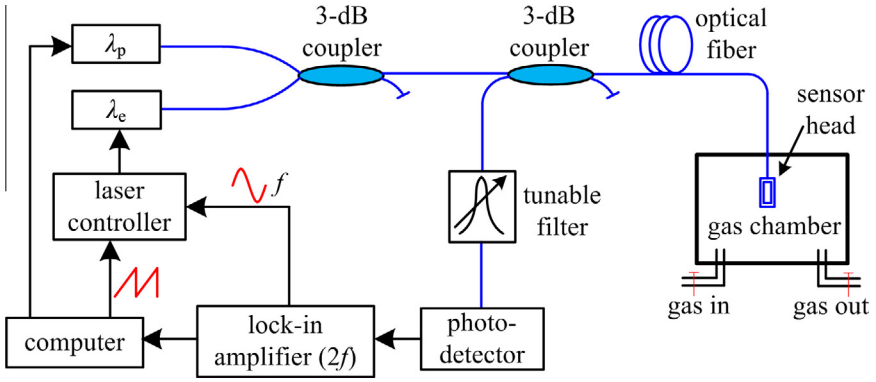

Fig. 26. An all-fiber gas sensor in which PA excitation and detection are performed within the same miniature fiber-tip cavity [41].

cable are shared by a number of sensors. Culshaw et al. reported a direct-absorption spatial division multiplexing system of 60 sensors for methane gas monitoring [125]. The system covers a measurement range from <100 ppm to 100% gas concentration (by volume) and was field tested at a landfill site. Ho et al. studied time division multiplexing of similar gas sensors [126] and concluded it is possible to multiplex up to 90 sensors in a ladder type network with a laser of 1 mW output power [127]. These multiplexed systems used gas cells with absorption path length from a few to 10 cm and achieved lower detection concentration level of less than 100 ppm. There are reports on multiplexed multi-point gas detection with intra-cavity and mode-locked lasers, however, the performances in terms of lower detection limit and the number of multiplexed sensors are inferior to the passive gas sensor network driven by an external laser [128,129].

As discussed in Section 2, SCFs and HC-PBGFs can be made to have sufficiently low loss and with side-openings, they can also be coiled to small diameters with very little additional loss. These elements would make it possible to develop smaller size gas sensors with performance better than the open-path sensors. With

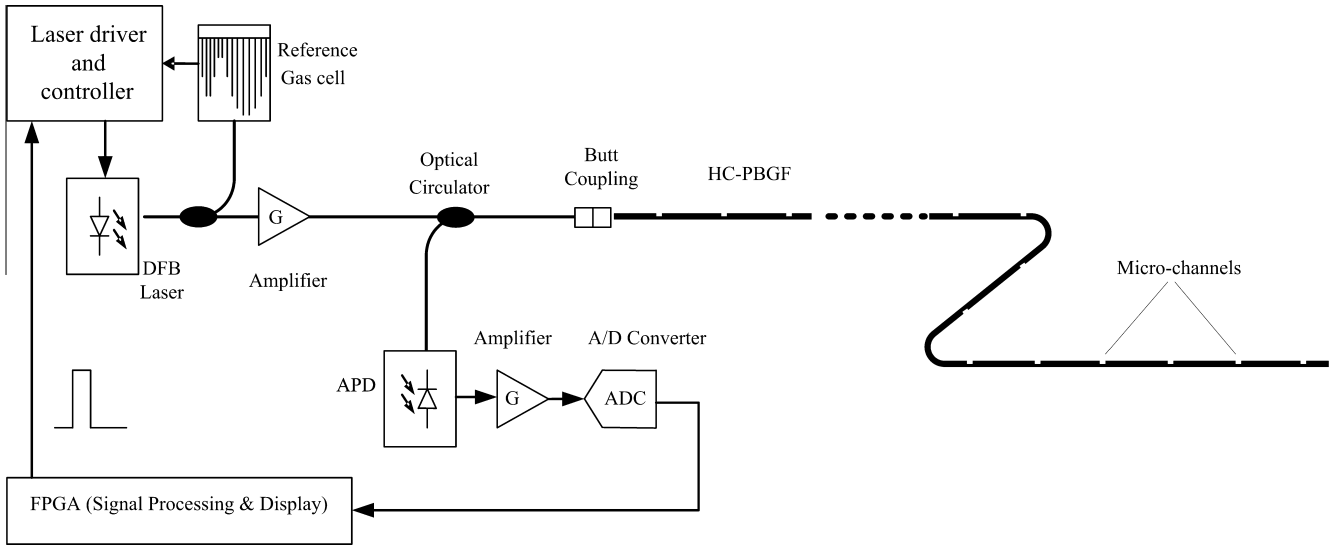

Fig. 27. Schematic of a distributed gas detection system based OTDR.

these all-fiber "point" sensors, it is possible to realize higher performance absorption-based fiber-optic gas sensor network by use of various multiplexing techniques [130,131] coupled with higher performance network components and better understanding of cross-talk and noise mechanisms.

With fiber-optic excitation and detection of PA pressure waves, it is also possible to realize PAS-based gas sensor networks. However, the situation is a slightly more complex for PAS-based sensors since two fiber-optic systems (PA excitation and acoustic wave detection) are involved and optimization of both systems in a coordinated matter would enable best overall performance of the gas detection system.

4.2. Distributed gas detection with optical fibers

Capability of distributed sensing is absolutely a superiority of fiber optic sensors over other conventional sensors. A truly distributed sensor should able to sense at least one measurand along its entire length which may replace a number of point sensors. Distributed strain and temperature sensing using SMF-based Rayleigh, Raman and Brillouin scattering has been well developed [132]. However, distributed gas detection with optical fiber was rarely reported. Sumida et al. [133] demonstrated distributed measurement of hydrogen with multimode optical fibers coated with platinum-supported tungsten trioxide (Pt/WO_3) film as hydrogen sensitive cladding and optical time domain reflectomotry (OTDR) to determine the spatial location. Wang et al. [134] reported distributed hydrogen sensing based on an acoustically induced transient and traveling long periodic grating in a platinum coated SMF. These sensors rely on particular coating materials and a truly distributed sensor based on gas absorption has not been reported to our knowledge, probably due to the lack of suitable waveguides.

IG-PCFs, SCFs and HC-PBGFs may be potential sensing elements for absorption-based distributed gas sensors. Gas and light interac-

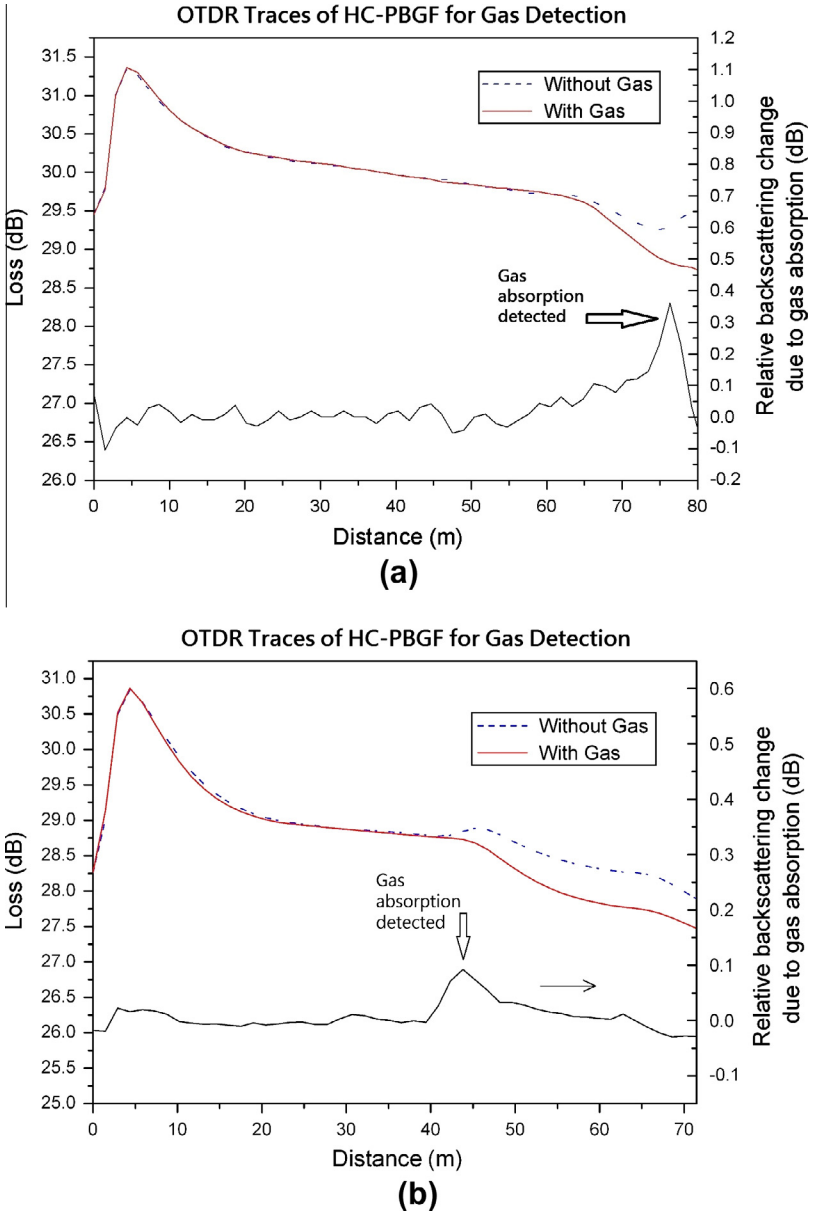

Fig. 28. Results of distributed gas measurement with 75 m long HC-PBGF. (a) 10% acetylene was filled from the end of the HC-PBGF and (b) 10% acetylene was filled at 44 m of the HC-PBGF.

tion takes place within the hole-columns where a large fraction of optical mode power exists. The gas concentration information along the fiber may be extracted by measuring the intensity change of back-reflected light by use of OTDR or other techniques. Lehmann et al. [135] reported a 7.5-m long fiber chain made by connecting two pieces of HC-PBGF sensing fibers to SMFs and, with white light spectroscopy and multi component analysis, they demonstrated discrimination of several different gases in a gas mixture. However, the system operated in a transmission mode, and detailed spatial information along the fiber cannot be determined.

We have carried out preliminary tests of a distributed gas detection system with a continuous length of HC-PBGF. Fig. 27 shows the schematic of the system. It consists of a 75 m long HC-PBGF (the sensing fiber), a pulsed high power DFB laser and an OTDR module. The DFB laser operates at 1531 nm which can be used to detect ammonia or acetylene. The DFB laser sends a high power optical pulse into the sensing fiber. As the pulse travels along the fiber, a small portion of the pulse's energy returns to the detector due to back-reflections from the fiber joints and back-scattering from the fiber itself. The pulse duration is ~10 ns, corresponding to a spatial resolution of 1 m. A large number of acquisitions (up to 64,000 times) can be performed and averaged in a second to provide a clear picture of the back scattering signal or loss profile of the fiber as a function of time, which is then converted into the distance along the fiber. To avoid saturating the APD, the Fresnel back-reflection at the joint between the SMF and the sensing HC-PBGF is reduced by butt coupling the HC-PBGF to an angle-cleaved SMF.

Along the 75 m HC-PBGF, a number of micro-channels were introduced. The separation between the micro-channels is about 1 m. To test the system, specific fiber segment with micro-channel(s) was put into the gas chamber within which test gas is filled. Fig. 28(a) shows the measured result when a fiber segment at the end of the 75 m HC-PBGF was put into the gas chamber in which 10% acetylene was filled. Fig. 28(b) shows the measured result when a fiber segment with a micro-channel at 44 m of the 75 m HC-PBGF was put into the acetylene-filled gas chamber. The loss induced by gas absorption can be seen by comparing the OTDR traces with and without gas. The lower curves show the computed difference between the slopes of the two OTDR traces (the black line) by which the locations and relative changes in backscattered signal due to gas absorption can be observed more clearly.

It should be pointed out that this is the first demonstration of distributed fiber gas sensor based on direct absorption spectroscopy. The system performance is expected to improve with the development of hollow-core fiber technology and the application of advanced source and signal processing techniques. To develop practical distributed sensors, the following key issues may need to be addressed:

(i) Development of high quality true single mode hollow-core fibers. Current commercial HC-PBGF fibers (HC-1550-02) actually supports several guided modes, and the coherent mode mixing or interference was identified as a major error source that affects the stability and noise performance of the sensors. Development of true single mode fiber, preferably single mode single polarization fiber would minimize such effects.

(ii) Development of advanced source and signal processing techniques. Compared with conventional OTDR systems, the source laser wavelength needs to be either locked to or tuned across the narrow absorption line of target gas. WMS may also be needed if higher detection sensitivity is desired. This will increase the complexity of the source systems, and the data created will also increase dramatically due to the addition of the extra dimension, i.e., the wavelength variable. Advanced signal processing may be needed to extract the useful information of gas concentration as function of distance along the optical fiber. Detection of multiple gas species is possible but at the expenses multiple laser sources or a tunable laser source, as well as increased load of data processing. Advanced signal processing may also help to reduce the effect of unwanted interferometric signals as mentioned in (i).

5. Conclusion

Direct absorption open path sensors with fiber pigtailed micro-optic cells have limitations in achieving higher sensitivity due to difficulty in fabricating long path length absorption cells with compact size. Silica based HC-PBGFs, SCFs and IG-PCFs enable gas-light interaction within their hole-columns over long distance and hence have potential for higher sensitivity gas detection. These fibers can be coiled to small diameter with little loss and hence can be used to make compact all-fiber gas sensors without the need of precision optical alignment.

A number of issues such as introduction of side-openings to speed up the response and proper packaging to prevent external contamination but allow gas to penetrate into the hole-columns, need to be addressed before practical sensors could be developed. Attempts have been made to fabricate side-openings or holes on various fibers but fabrication of a large number of side-holes along a long fiber is a practical challenge.

Current SCFs and HC-PBGFs support more than one guided mode. Since typically laser sources are needed to match to the narrow gas absorption lines, mode mixing or interference effect is another source of noise that needs to be minimized. The introduction of side-holes could induce mode/polarization coupling and worsen the situation. Wavelength/phase modulation and advanced digital signal processing may be used to minimize the effect but more work is needed to prove the effectiveness of the methods.

With SCFs and HC-PBGFs, distributed gas detection may be achieved. A demonstration of OTDR-based distributed methane detection with 75-m long HC-PBGF was demonstrated, but the results are still very preliminary and much more work is needed to optimize the source, detection and signal processing unit, as well as the sensing fiber cable, in order to develop a practical distributed gas detection system. Coupled with advanced tunable laser sources, multi components gas detection is possible.

For PAS-based gas sensors, very high sensitivity of the order of ppb has been experimentally demonstrated. Attempts are being made to develop practical fiber-optic acoustic probes and interrogation units, with which all-fiber PAS-based gas sensors may be developed as well as lower cost PAS-based multiplexed or distributed gas sensor networks.

Acknowledgments

We acknowledge the support of the National Natural Science Foundation of China (NSFC) through Grant No. 61290313; the Hong Kong Special Administrative Region Government through GRF Grants PolyU 5177/10E and PolyU 5096/09E, and ITC Grants ITS/548/09 and ITS/054/06; as well as the Hong Kong Polytechnic University through Grant J-BB9K and 4ZZ-E1.

References

[1] C.N. Banwell, E. McCash, Fundamentals of Molecular Spectroscopy, McGraw-Hill Book, London, New York, 1994.
[2] H. Inaba, T. Kobayasi, M. Hirama, M. Hamza, Optical-fibre network system for air-pollution monitoring over a wide area by optical absorption method, Electron. Lett. 15 (1979) 749–751.

[3] G. Stewart, C. Tandy, D. Moodie, M.A. Morante, F. Dong, Design of a fibre optic multi-point sensor for gas detection, Sensor Actuat. B – Chem. 51 (1998) 227–232.
[4] S.D. Schwab, R.L. McCreery, Remote, long-pathlength cell for high-sensitivity raman spectroscopy, Appl. Spectrosc. 41 (1987) 126–130.
[5] M.P. Buric, K.P. Chen, J. Falk, S.D. Woodruff, Enhanced spontaneous Raman scattering and gas composition analysis using a photonic crystal fiber, Appl. Opt. 47 (2008) 4255–4261.
[6] Y. Xuan, A.S.P. Chang, C. Bin, C. Gu, T.C. Bond, Multiplexed gas sensing based on Raman spectroscopy in photonic crystal fiber, Photonics Conf. (IPC) IEEE 2012 (2012) 447–448.
[7] X. He, G.A. Rechnitz, Linear response function for fluorescence-based fiber-optic CO_2 sensors, Anal. Chem. 67 (1995) 2264–2268.
[8] C.S. Chu, Y.L. Lo, T.W. Sung, Review on recent developments of fluorescent oxygen and carbon dioxide optical fiber sensors, Photonics Sens. 1 (2011) 234–250.
[9] C. Nylander, B. Liedberg, T. Lind, Gas detection by means of surface plasmon resonance, Sensor Actuat. 3 (1982) 79–88.
[10] A. Abdelghani, J.M. Chovelon, N. Jaffrezic-Renault, C. Ronot-Trioli, C. Veillas, H. Gagnaire, Surface plasmon resonance fibre-optic sensor for gas detection, Sensor Actuat. B: Chem. 39 (1997) 407–410.
[11] B. Lee, S. Roh, J. Park, Current status of micro- and nano-structured optical fiber sensors, Opt. Fiber Technol. 15 (2009) 209–221.
[12] M.A. Butler, D.S. Ginley, Hydrogen sensing with palladium-coated optical fiber, J. Appl. Phys. 64 (1988) 3706–3712.
[13] B. Sutapun, M. Tabib-Azar, A. Kazemi, Pd-coated elastooptic fiber optic Bragg grating sensors for multiplexed hydrogen sensing, Sensor Actuat. B: Chem. 60 (1999) 27–34.
[14] J. Dakin, P. Chambers, Review of methods of optical gas detection by direct optical spectroscopy, with emphasis on correlation spectroscopy, in: F. Baldini, A.N. Chester, J. Homola, S. Martellucci (Eds.), Optical Chemical Sensors, Springer, Netherlands, 2006, pp. 457–477.
[15] B. MacCraith, Optical fiber chemical sensor systems and devices, in: K.T.V. Grattan, B.T. Meggitt (Eds.), Optical Fiber Sensor Technology, Springer, Netherlands, 1999, pp. 15–46.
[16] G. Korotcenkov, Chemical Sensors: Fundamentals of Sensing Materials, Momentum Press, New York, 2010.
[17] J. Dakin, B. Culshaw, Optical Fiber Sensors, Artech House, Boston, 1988.
[18] J.U. White, Very long optical paths in air, J. Opt. Soc. Am. 66 (1976) 411–416.
[19] D. Herriott, H.J. Schulte, Folded optical delay lines, Appl. Opt. 4 (1965) 883–889.
[20] G. Stewart, F.A. Muhammad, B. Culshaw, Sensitivity improvement for evanescent-wave gas sensors, Sensor Actuat. B: Chem. 11 (1993) 521–524.
[21] S. Sudo, I. Yokohama, H. Yasaka, Y. Sakai, T. Ikegami, Optical fiber with sharp optical absorptions by vibrational-rotational absorption of C_2H_2 molecules, IEEE Photonics Technol. Lett. 2 (1990) 128–131.
[22] J.C. Knight, T.A. Birks, P.S.J. Russell, D.M. Atkin, All-silica single-mode optical fiber with photonic crystal cladding, Opt. Lett. 21 (1996) 1547–1549.
[23] T.A. Birks, J.C. Knight, P.S. Russell, Endlessly single-mode photonic crystal fiber, Opt. Lett. 22 (1997) 961–963.
[24] J. Ju, W. Jin, M.S. Demokan, Two-mode operation in highly birefringent photonic crystal fiber, Photonics Technol. Lett. IEEE 16 (2004) 2472–2474.
[25] A. Ferrando, E. Silvestre, P. Andres, J.J. Miret, M.V. Andres, Designing the properties of dispersion-flattened photonic crystal fibers, Opt. Express 9 (2001) 687–697.
[26] V. Finazzi, T.M. Monro, D.J. Richardson, Small-core silica holey fibers: nonlinearity and confinement loss trade-offs, J. Opt. Soc. Am. B – Opt. Phys. 20 (2003) 1427–1436.
[27] K. Saitoh, M. Koshiba, Highly nonlinear dispersion-flattened photonic crystal fibers for supercontinuum generation in a telecommunication window, Opt. Express 12 (2004) 2027–2032.
[28] T.M. Monro, H. Ebendorff-Heidepriem, Progress in microstructured optical fibers, Annual Review of Materials Research, Annual Reviews, Palo Alto, 2006, pp. 467–495.
[29] T.M. Monro, D.J. Richardson, P.J. Bennett, Developing holey fibres for evanescent field devices, Electron. Lett. 35 (1999) 1188–1189.
[30] Y.L. Hoo, W. Jin, H.L. Ho, D.N. Wang, R.S. Windeler, Evanescent-wave gas sensing using microstructure fiber, Opt. Eng. 41 (2002) 8–9.
[31] Y.L. Hoo, W. Jin, C.Z. Shi, H.L. Ho, D.N. Wang, S.C. Ruan, Design and modeling of a photonic crystal fiber gas sensor, Appl. Opt. 42 (2003) 3509–3515.
[32] Y.L. Hoo, W. Jin, H.L. Ho, J. Ju, D.N. Wang, Gas diffusion measurement using hollow-core photonic bandgap fiber, Sensor Actuat. B – Chem. 105 (2005) 183–186.
[33] T. Ritari, J. Tuominen, H. Ludvigsen, J.C. Petersen, T. Sorensen, T.P. Hansen, H.R. Simonsen, Gas sensing using air-guiding photonic bandgap fibers, Opt. Express 12 (2004) 4080–4087.
[34] G. Pickrell, W. Peng, A. Wang, Random-hole optical fiber evanescent-wave gas sensing, Opt. Lett. 29 (2004) 1476–1478.
[35] A.S. Webb, F. Poletti, D.J. Richardson, and J.K. Sahu, Suspended-core holey fiber for evanescent-field sensing. Optical Engineering 46 (2007).
[36] A. Schmohl, A. Miklos, P. Hess, Detection of ammonia by photoacoustic spectroscopy with semiconductor lasers, Appl. Opt. 41 (2002) 1815–1823.
[37] M.B. Pushkarsky, M.E. Webber, C.K.N. Patel, Ultra-sensitive ambient ammonia detection using CO_2-laser-based photoacoustic spectroscopy, Appl. Phys. B – Lasers Opt. 77 (2003) 381–385.
[38] A.A. Kosterev, Y.A. Bakhirkin, R.F. Curl, F.K. Tittel, Quartz-enhanced photoacoustic spectroscopy, Opt. Lett. 27 (2002) 1902–1904.
[39] T. Laurila, H. Cattaneo, V. Koskinen, J. Kauppinen, R. Hernberg, Diode laser-based photoacoustic spectroscopy with interferometrically-enhanced cantilever detection, Opt. Express 13 (2005) 2453–2458.
[40] Q.Y. Wang, J.W. Wang, L.A. Li, Q.X. Yu, An all-optical photoacoustic spectrometer for trace gas detection, Sensor Actuat. B – Chem. 153 (2011) 214–218.
[41] Y. Cao, W. Jin, H.L. Ho, J. Ma, Miniature fiber-tip photoacoustic spectrometer for trace gas detection, Opt. Lett. 38 (2013) 434–436.
[42] F.P. Bernath, Spectra of Atoms and Molecules, Oxford University Press, New York, 2005.
[43] S. Svanberg, Atomic and Molecular Spectroscopy: Basic Aspects and Practical Applications, Springer, Berlin, 2004.
[44] B. Culshaw, G. Stewart, F. Dong, C. Tandy, D. Moodie, Fibre optic techniques for remote spectroscopic methane detection – from concept to system realisation, Sensor Actuat. B – Chem. 51 (1998) 25–37.
[45] G. Whitenett, G. Stewart, H.B. Yu, B.N. Culshaw, Investigation of a tuneable mode-locked fiber laser for application to multipoint gas spectroscopy, J. Lightwave Technol. 22 (2004) 813–819.
[46] J. Reid, D. Labrie, 2nd harmonic detection with tunable diode lasers – comparison of experiment and theory, Appl. Phys. B 26 (1981) 203–210.
[47] H.L. Ho, W. Jin, M.S. Demokan, Quantitative measurement of acetylene by using external-cavity tunable diode laser, in: Proc. SPIE 3852, Harsh Environment Sensors II, Boston, US, 1999, pp. 124–133.
[48] G. Stewart, A. Mencaglia, W. Philp, W. Jin, Interferometric signals in fiber optic methane sensors with wavelength modulation of the DFB laser source, J. Lightwave Technol. 16 (1998) 43–53.
[49] W. Jin, G. Stewart, W. Philp, B. Culshaw, M.S. Demokan, Limitation of absorption-based fiber optic gas sensors by coherent reflections, Appl. Opt. 36 (1997) 6251–6255.
[50] W. Jin, Y.Z. Xu, M.S. Demokan, G. Stewart, Investigation of interferometric noise in fiber-optic gas sensors with use of wavelength modulation spectroscopy, Appl. Opt. 36 (1997) 7239–7246.
[51] M.A. Morante, G. Stewart, B. Culshaw, J.M. LopezHiguera, New micro-optic cell for optical fibre gas sensors with interferometric noise reduction, Electron. Lett. 33 (1997) 1407–1409.
[52] J.M. Sa, Y.P. Chen, G. Zhang, Z. Zhou, L.J. Cui, Gas cell based on cascaded GRIN lens for optical fiber gas sensor, in: 3rd International Symposium on Advanced Optical Manufacturing and Testing Technologies: Optical Test and Measurement Technology and Equipment, Parts 1–3, vol. 6723, 2007, Article No. 67234I.
[53] H.L. Ho, J. Ju, W. Jin, Fiber optic gas detection system for health monitoring of oil-filled transformer, in: Proc. SPIE 7503, 20th International Conference on Optical Fibre Sensors, Edinburgh, United Kingdom, 2009, Article No. 75030T.
[54] D. Liu, S.N. Fu, M. Tang, P. Shum, D.M. Liu, Comb filter-based fiber-optic methane sensor system with mitigation of cross gas sensitivity, J. Lightwave Technol. 30 (2012) 3103–3109.
[55] V. Ruddy, An effective attenuation coefficient for evanescent wave spectroscopy using multimode fiber, Fiber Integr. Opt. 9 (1990) 143–151.
[56] G. Stewart, B. Culshaw, Optical waveguide modelling and design for evanescent field chemical sensors, Opt. Quant. Electron. 26 (1994) 249–259.
[57] G. Stewart, J. Norris, D.F. Clark, B. Culshaw, Evanescent-wave chemical sensors – a theoretical evaluation, Int. J. Optoelectron. 6 (1991) 227–238.
[58] C.D. Hussey, J.D. Minelly, Optical fibre polishing with a motor-driven polishing wheel, Electron. Lett. 24 (1988) 805–807.
[59] G. Brambilla, V. Finazzi, D. Richardson, Ultra-low-loss optical fiber nanotapers, Opt. Express 12 (2004) 2258–2263.
[60] G. Brambilla, Optical fibre nanotaper sensors, Opt. Fiber Technol. 16 (2010) 331–342.
[61] G. Stewart, W. Jin, B. Culshaw, Prospects for fibre-optic evanescent-field gas sensors using absorption in the near-infrared, Sensor Actuat. B – Chem. 38 (1997) 42–47.
[62] W. Jin, G. Stewart, B. Culshaw, S. Murray, M. Wilkinson, J.O.W. Norris, Performance limitation of fiber optic methane sensors due to interference effects, J. Lightwave Technol. 14 (1996) 760–769.
[63] F.A. Muhammad, G. Stewart, W. Jin, Sensitivity enhancement of D-fiber methane gas sensor using high-index overlay, IEE Proc. – J. Optoelectron. 140 (1993) 115–118.
[64] H.L. Ho, Y.L. Hoo, W. Jin, J. Ju, D.N. Wang, R.S. Windeler, Q. Li, Optimizing microstructured optical fibers for evanescent wave gas sensing, Sensor Actuat. B – Chem. 122 (2007) 289–294.
[65] L. Xiao, M.S. Demokan, W. Jin, Y. Wang, C.L. Zhao, Fusion splicing photonic crystal fibers and conventional single-mode fibers: microhole collapse effect, J. Lightwave Technol. 25 (2007) 3563–3574.
[66] P. Kaiser, H.W. Astle, Low-loss single-material fibers made from pure fused silica, Bell Syst. Tech. J. 53 (1974) 1021–1039.
[67] T.M. Monro, S. Warren-Smith, E.P. Schartner, A. Francois, S. Heng, H. Ebendorff-Heidepriem, S. Afshar, Sensing with suspended-core optical fibers, Opt. Fiber Technol. 16 (2010) 343–356.
[68] S. Selleri, E. Coscelli, M. Sozzi, A. Cucinotta, F. Poli, D. Passaro, Air-suspended solid-core fibers for sensing, in: Proc. SPIE 7356, Optical Sensors Prague, Czech Republic, 2009, Article No. 73561L.
[69] C.M.B. Cordeiro, M.A.R. Franco, C.J.S. Matos, F. Sircilli, V.A. Serrao, C.H.B. Cruz, Single-design-parameter microstructured optical fiber for chromatic

dispersion tailoring and evanescent field enhancement, Opt. Lett. 32 (2007) 3324–3326.
[70] T.M. Monro, D.J. Richardson, N.G.R. Broderick, P.J. Bennett, Modeling large air fraction holey optical fibers, J. Lightwave Technol. 18 (2000) 50–56.
[71] A. van Brakel, C. Grivas, M.N. Petrovich, D.J. Richardson, Micro-channels machined in microstructured optical fibers by femtosecond laser, Opt. Express 15 (2007) 8731–8736.
[72] F.M. Cox, R. Lwin, M.C.J. Large, C.M.B. Cordeiro, Opening up optical fibres, Opt. Express 15 (2007) (1848) 11843–11848.
[73] S.C. Warren-Smith, H. Ebendorff-Heidepriem, T.C. Foo, R. Moore, C. Davis, T.M. Monro, Exposed-core microstructured optical fibers for real-time fluorescence sensing, Opt. Express 17 (2009) 18533–18542.
[74] R. Kostecki, H. Ebendorff-Heidepriem, C. Davis, G. McAdam, S.C. Warren-Smith, T.M. Monro, Silica exposed-core microstructured optical fibers, Opt. Mater. Express 2 (2012) 1538–1547.
[75] J. Chen, A. Hangauer, R. Strzoda, T.G. Euser, J.S.Y. Chen, M. Scharrer, P.S.J. Russell, M.C. Amann, Sensitivity limits for near-infrared gas sensing with suspended-core PCFs directly coupled with VCSELs, in: Conference on Lasers and Electro-Optics (CLEO) and Quantum Electronics and Laser Science Conference (QELS), 2010.
[76] L. Dong, B.K. Thomas, L.B. Fu, Highly nonlinear silica suspended core fibers, Opt. Express 16 (2008) 16423–16430.
[77] P. Russell, Photonic crystal fibers, Science 299 (2003) 358.
[78] R.F. Cregan, B.J. Mangan, J.C. Knight, T.A. Birks, P.S. Russell, P.J. Roberts, D.C. Allan, Single-mode photonic band gap guidance of light in air, Science 285 (1999) 1537–1539.
[79] C.M. Smith, N. Venkataraman, M.T. Gallagher, D. Muller, J.A. West, N.F. Borrelli, D.C. Allan, K.W. Koch, Low-loss hollow-core silica/air photonic bandgap fibre, Nature 424 (2003) 657–659.
[80] P.J. Roberts, F. Couny, H. Sabert, B.J. Mangan, D.P. Williams, L. Farr, M.W. Mason, A. Tomlinson, T.A. Birks, J.C. Knight, P.S.J. Russell, Ultimate low loss of hollow-core photonic crystal fibres, Opt. Express 13 (2005) 236–244.
[81] NKT Photonics A/S. <http://www.nktphotonics.com>.
[82] Datasheet of HC-1550-02, NKT Photonics A/S. <http://www.nktphotonics.com>.
[83] J. Henningsen, J. Hald, Dynamics of gas flow in hollow core photonic bandgap fibers, Appl. Opt. 47 (2008) 2790–2797.
[84] R.M. Wynne, B. Barabadi, K.J. Creedon, A. Ortega, Sub-minute response time of a hollow-core photonic bandgap fiber gas sensor, J. Lightwave Technol. 27 (2009) 1590–1596.
[85] J.P. Parry, B.C. Griffiths, N. Gayraud, E.D. McNaghten, A.M. Parkes, W.N. MacPherson, D.P. Hand, Towards practical gas sensing with micro-structured fibres, Meas. Sci. Technol. 20 (2009) 075301.
[86] J.P. Carvalho, H. Lehmann, H. Bartelt, F. Magalhaes, R. Amezcua-Correa, J.L. Santos, J.V. Roosbroeck, F.M. Araujo, L.A. Ferreira, J.C. Knight, Remote system for detection of low-levels of methane based on photonic crystal fibres and wavelength modulation spectroscopy, J. Sensor 2009 (2009) 398403.
[87] H. Lehmann, S. Bruckner, J. Kobelke, G. Schwotzer, K. Schuster, R. Willsch, Toward photonic crystal fiber based distributed chemosensors, in: SPIE Proc., 17th International Conference on Optical Fibre Sensors, vol. 5855, Bellingham, 2005, pp. 419–422.
[88] C.M.B. Cordeiro, E.M. dos Santos, C.H.B. Cruz, C.J.S. de Matos, D.S. Ferreira, Lateral access to the holes of photonic crystal fibers – selective filling and sensing applications, Opt. Express 14 (2006) 8403–8412.
[89] X.F. Li, J. Pawlat, J.X. Liang, G. Xu, T. Ueda, Fabrication of photonic bandgap fiber gas cell using focused ion beam cutting, Jpn. J. Appl. Phys. 48 (2009) 06FK05.
[90] X.F. Li, J.X. Liang, H. Oigawa, T. Ueda, Doubled optical path length for photonic bandgap fiber gas cell using micromirror, Jpn. J. Appl. Phys. 50 (2011) 06GM01.
[91] D.N. Wang, Micro-engineered optical fiber sensors fabricated by femtosecond laser micromachining, Optical Sensors, Optical Society of America, Monterey, California, USA, 2012, pp. STu4F.1.
[92] Y. Lai, K. Zhou, L. Zhang, I. Bennion, Microchannels in conventional single-mode fibers, Opt. Lett. 31 (2006) 2559–2561.
[93] C.J. Hensley, D.H. Broaddus, C.B. Schaffer, A.L. Gaeta, Photonic band-gap fiber gas cell fabricated using femtosecond micromachining, Opt. Express 15 (2007) 6690–6695.
[94] W. Jin, L. Qi, H.L. Ho, Y. Cao, Gas detection with micro and nano-engineered optical fibers, Optical Sensors, Optical Society of America, Monterey, California, USA, 2012, pp. STu4F.3.
[95] Y.L. Hoo, S.J. Liu, H.L. Ho, W. Jin, Fast response microstructured optical fiber methane sensor with multiple side-openings, IEEE Photonics Technol. Lett. 22 (2010) 296–298.
[96] A. Elia, P.M. Lugara, C. Di Franco, V. Spagnolo, Photoacoustic techniques for trace gas sensing based on semiconductor laser sources, Sensors 9 (2009) 9616–9628.
[97] J. Li, W. Chen, B. Yu, Recent progress on infrared photoacoustic spectroscopy techniques, Appl. Spectrosc. Rev. 46 (2011) 440–471.
[98] C. Haisch, Photoacoustic spectroscopy for analytical measurements, Meas. Sci. Technol. 23 (2012) 012001 (17pp).
[99] T. Schmid, Photoacoustic spectroscopy for process analysis, Anal. Bioanal. Chem. 384 (2006) 1071–1086.
[100] Y.C. Cao, W. Jin, L.H. Ho, Z.B. Liu, Evanescent-wave photoacoustic spectroscopy with optical micro/nano fibers, Opt. Lett. 37 (2012) 214–216.
[101] C. Wang, W. Jin, J. Ma, Y. Wang, H.L. Ho, X. Shi, Suspended-core photonic micro-cells for sensing and device applications, Opt. Lett. 38 (2013) 1881–1883.
[102] S. Schilt, L. Thevenaz, M. Nikles, L. Emmenegger, C. Huglin, Ammonia monitoring at trace level using photoacoustic spectroscopy in industrial and environmental applications, Spectrochim. Acta Part A – Mol. Biomol. Spectrosc. 60 (2004) 3259–3268.
[103] M.E. Webber, M. Pushkarsky, C.K.N. Patel, Fiber-amplifier-enhanced photoacoustic spectroscopy with near-infrared tunable diode lasers, Appl. Opt. 42 (2003) 2119–2126.
[104] J.P. Besson, S. Schilt, E. Rochat, L. Thevenaz, Ammonia trace measurements at ppb level based on near-IR photoacoustic spectroscopy, Appl. Phys. B – Laser Opt. 85 (2006) 323–328.
[105] A.A. Kosterev, F.K. Tittel, D.V. Serebryakov, A.L. Malinovsky, I.V. Morozov, Applications of quartz tuning forks in spectroscopic gas sensing, Rev. Sci. Instrum. 76 (2005) 043105.
[106] R. Lewicki, G. Wysocki, A.A. Kosterev, F.K. Tittel, Carbon dioxide and ammonia detection using 2 mu m diode laser based quartz-enhanced photoacoustic spectroscopy, Appl. Phys. B – Laser Opt. 87 (2007) 157–162.
[107] S. Schilt, A.A. Kosterev, F.K. Tittel, Performance evaluation of a near infrared QEPAS based ethylene sensor, Appl. Phys. B – Lasers Opt. 95 (2009) 813–824.
[108] M.H. de Paula, A.A. de Carvalho, C.A. Vinha, N. Cella, H. Vargas, Optical microphone for photoacoustic-spectroscopy, J. Appl. Phys. 64 (1988) 3722–3724.
[109] M.H. de Paula, C.A. Vinha, R.G. Badini, High-sensitivity optical microphone for photoacoustics, Rev. Sci. Instrum. 63 (1992) 3487–3491.
[110] M.H. de Paula, A.R. Omido, D.F.D. Schumaher, H.H. da Gama, Optical microphone: new results, Rev. Sci. Instrum. 75 (2004) 2863–2864.
[111] K. Wilcken, J. Kauppinen, Optimization of a microphone for photoacoustic spectroscopy, Appl. Spectrosc. 57 (2003) 1087–1092.
[112] V. Koskinen, J. Fonsen, K. Roth, J. Kauppinen, Progress in cantilever enhanced photoacoustic spectroscopy, Vib. Spectrosc. 48 (2008) 16–21.
[113] M. Kohring, A. Pohlkotter, U. Willer, M. Angelmahr, W. Schade, Tuning fork enhanced interferometric photoacoustic spectroscopy: a new method for trace gas analysis, Appl. Phys. B – Lasers Opt. 102 (2011) 133–139.
[114] M. Kohring, U. Willer, S. Bottger, A. Pohlkotter, W. Schade, Fiber-coupled ozone sensor based on tuning fork-enhanced interferometric photoacoustic spectroscopy, IEEE J. Sel. Top. Quantum Electron. 18 (2012) 1566–1572.
[115] D.H. Leslie, G.L. Trusty, A. Dandridge, T.G. Giallorenzi, Fibre-optic spectrophone, Electron. Lett. 17 (1981) 581–582.
[116] J. Breguet, J.P. Pellaux, N. Gisin, Photoacoustic detection of trace gases with an optical microphone, Sensor Actuat. A – Phys. 48 (1995) 29–35.
[117] Y. Kawabata, K. Yasunaga, T. Imasaka, N. Ishibashi, Photoacoustic spectrometry using a fiberoptic pressure sensor, Anal. Chem. 65 (1993) 3493–3496.
[118] P.C. Beard, F. Perennes, E. Draguioti, T.N. Mills, Optical fiber photoacoustic–photothermal probe, Opt. Lett. 23 (1998) 1235–1237.
[119] O.C. Akkaya, O. Kilic, M.J.F. Digonnet, G.S. Kino, O. Solgaard, High-sensitivity thermally stable acoustic fiber sensor, Sensor IEEE 2010 (2010) 1148–1151.
[120] F. Xu, D.X. Ren, X.L. Shi, C. Li, W.W. Lu, L. Lu, L. Lu, B.L. Yu, High-sensitivity Fabry–Perot interferometric pressure sensor based on a nanothick silver diaphragm, Opt. Lett. 37 (2012) 133–135.
[121] F.W. Guo, T. Fink, M. Han, L. Koester, J. Turner, J.S. Huang, High-sensitivity, high-frequency extrinsic Fabry–Perot interferometric fiber-tip sensor based on a thin silver diaphragm, Opt. Lett. 37 (2012) 1505–1507.
[122] J. Ma, W. Jin, H.L. Ho, J.Y. Dai, High-sensitivity fiber-tip pressure sensor with graphene diaphragm, Opt. Lett. 37 (2012) 2493–2495.
[123] J. Ma, H. Xuan, H.L. Ho, W. Jin, Y. Yang, S. Fan, A fiber-optic Fabry–Perot acoustic sensor with multi-layer graphene diaphragm, IEEE Photonics Technol. Lett. 99 (2013) 1.
[124] V. Koskinen, J. Fonsen, K. Roth, J. Kauppinen, Cantilever enhanced photoacoustic detection of carbon dioxide using a tunable diode laser source, Appl. Phys. B – Lasers Opt. 86 (2007) 451–454.
[125] B. Culshaw, A. Kersey, Fiber-optic sensing: a historical perspective, J. Lightwave Technol. 26 (2008) 1064–1078.
[126] H.L. Ho, W. Jin, M.S. Demokan, Sensitive, multipoint gas detection using TDM and wavelength modulation spectroscopy, Electron. Lett. 36 (2000) 1191–1193.
[127] H.L. Ho, Multi-point Fiber Optic Gas Sensor Systems, PhD Thesis, The Hong Kong Polytechnic University, Hong Kong, 2002.
[128] Y. Zhang, W. Jin, H.B. Yu, M. Zhang, Y.B. Liao, H.L. Ho, M.S. Demokan, G. Stewart, B. Culshaw, Y.H. Li, Novel intracavity sensing network based on mode-locked fiber laser, IEEE Photonics Technol. Lett. 14 (2002) 1336–1338.
[129] G. Stewart, H.B. Yu, G. Whitenett, B. Culshaw, A mode-locked fibre laser system for multi-point intra-cavity gas spectroscopy, in: Proc. 15th Int. Conf. Optical Fiber Sensors (OFS-15), 2002, pp. 257–260.
[130] J.P. Dakin, Multiplexed and distributed optical fiber sensor systems, J. Phys. E – Sci. Instrum. 20 (1987) 954–967.
[131] A.D. Kersey, A. Dandridge, Distributed and multiplexed fibre-optic sensor systems, J. Inst. Electron. Radio Eng. 58 (1988) S99–S112.
[132] X. Bao, L. Chen, Recent progress in distributed fiber optic sensors, Sensors 12 (2012) 8601–8639.
[133] S. Sumida, S. Okazaki, S. Asakura, H. Nakagawa, H. Murayama, T. Hasegawa, Distributed hydrogen determination with fiber-optic sensor, Sensor Actuat. B – Chem. 108 (2005) 508–514.

[134] D.Y. Wang, Y.M. Wang, J.M. Gong, A.B. Wang, Fully distributed fiber-optic hydrogen sensing using acoustically induced long-period grating, IEEE Photonics Technol. Lett. 23 (2011) 733–735.
[135] H. Lehmann, H. Bartelt, R. Willsch, R. Amezcua-Correa, J.C. Knight, Distributed gas sensor based on a photonic bandgap fiber cell with laser-drilled, lateral micro channels, in: J.L. Santos, B. Culshaw, J.M. LopezHiguera, W.N. MacPherson (Eds.), Fourth European Workshop on Optical Fibre Sensors, 2010.